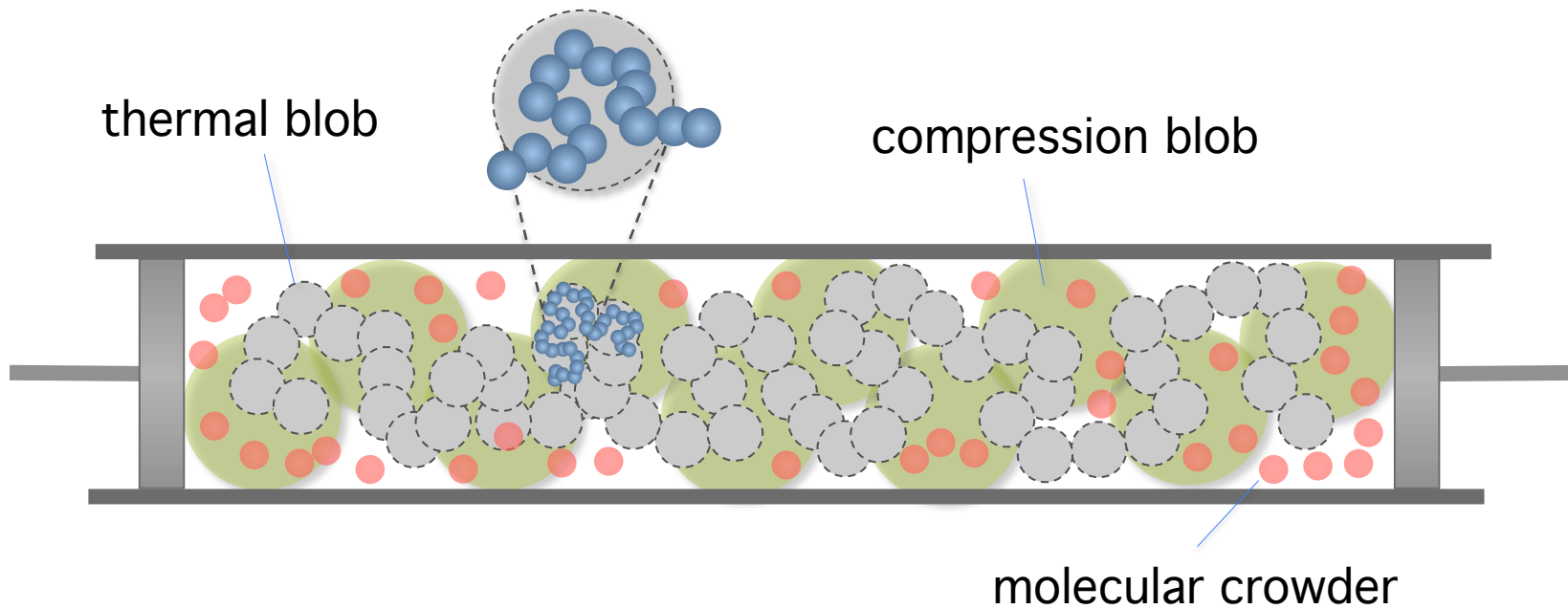




**Polymers under confinement: single polymers, how they interact, and as model chromosomes**

Journal:	<i>Soft Matter</i>
Manuscript ID:	SM-REV-12-2014-002734.R1
Article Type:	Review Article
Date Submitted by the Author:	31-Jan-2015
Complete List of Authors:	Ha, Bae-Yeun; University of Waterloo, Jung, Youngkyun; KISTI,



# Polymers under confinement: single polymers, how they interact, and as model chromosomes<sup>†</sup>

Bae-Yeun Ha<sup>a\*</sup> and Youngkyun Jung<sup>b\*</sup>

Received Xth XXXXXXXXXXXX 20XX, Accepted Xth XXXXXXXXXXXX 20XX

First published on the web Xth XXXXXXXXXXXX 200X

DOI: 10.1039/b000000x

How confinement or a physical constraint modifies polymer chains is not only a classical problem in polymer physics but also relevant in a variety of contexts such as single-molecule manipulations, nanofabrication in narrow pores, and modelling of chromosome organization. Here, we review recent progress in our understanding of polymers in a confined (and crowded) space. To this end, we highlight converging views of these systems from computational, experimental, and theoretical approaches, and then clarify what remains to be clarified. In particular, we focus on exploring how cylindrical confinement reshapes individual chains and induces segregation forces between them – by pointing to the relationships between intra-chain organization and chain segregation. In the presence of crowders, chain molecules can be entropically phase-separated into a condensed state. We include a kernel of discussions on the nature of chain compaction by crowders, especially in a confined space. Finally, we discuss the relevance of confined polymers for the nucleoid, an intracellular space in which the bacterial chromosome is tightly packed, in part by cytoplasmic crowders.

## 1 Introduction

Polymers are chain molecules consisting of many repeated subunits or monomers<sup>1–3</sup> (see Fig. 1). If biomolecules or biopolymers (e.g., DNA) are naturally-occurring ones, synthetic ones include polyethylene. Some of them carry electric charges in aqueous solution (e.g., polyvinyl sulfonic acid and many biopolymers)<sup>4</sup> or have nontrivial topologies or architectures, e.g., ring, star, branched, or cross-linked (see Fig. 1). Because of their flexibility, chain molecules store many internal degrees of freedom. The essence of this is well captured in the metaphor of these molecules as ‘freedom in chains,’<sup>5</sup> as illustrated in Fig. 1(a). Unlike other materials such as metals, the conformational entropy, associated with these degrees of freedom, often dominates their thermodynamic quantities such as chain elasticity and segregation.

Accordingly, polymers often behave as entropic objects. How they are modified by confinement or physical constraints is not only a classical problem in polymer physics<sup>1,2,6–8</sup> but also relevant in various contexts such as single-molecule manipulations or nanofabrication in narrow pores,<sup>9–18</sup> chromosome organization, especially in elongated bacterial

cells,<sup>19–23</sup> and viral DNA packing in a viral capsid or release into a host cell<sup>24,25</sup> (see the illustrations in Fig. 1(b)-(d)). For instance, in a recent experimental study, chromosomes released from lysed *E. coli* cells were manipulated mechanically and osmotically.<sup>14</sup> A confined polymer model proves to be useful for interpreting force-compression or osmotic compaction of the chromosomes.<sup>14</sup> This physical approach complements earlier results for single-chromosome organization, especially into (topologically-independent) structural units.<sup>26–28</sup>

In this review, we attempt to present several key results for polymers in a confined (and crowded) space in an effort to offer a coherent view of their single chain properties and the way they interact. Indeed, a set of converging results has recently emerged from computational, experimental, and theoretical approaches. In particular, we focus on exploring the benefits of cylindrical confinement in reshaping individual chains and inducing (entropic) segregation forces between them. For this, we discuss the relationships between intra-chain organization and chain segregation. Intriguingly, polymers can be compacted entropically in the presence of crowding particles. We include a kernel of discussions on the nature of chain compaction by crowders, highlighting the interplay between crowding and confinement effects. Finally, we discuss the relevance of confined polymers for the nucleoid, an intracellular space in which the bacterial chromosome is tightly packed, in part by cytoplasmic crowders.

Considering the availability of a few excellent reviews on

<sup>†</sup> Electronic Supplementary Information (ESI) available: [details of any supplementary information available should be included here]. See DOI: 10.1039/b000000x/

<sup>a</sup> Department of Physics and Astronomy, University of Waterloo, Waterloo, Ontario, Canada N2L 3G1. E-mail: [byha@uwaterloo.ca](mailto:byha@uwaterloo.ca)

<sup>b</sup> National Institute of Supercomputing and Networking, Korea Institute of Science and Technology Information, Daejeon 305-806, Korea. E-mail: [yjung@kisti.re.kr](mailto:yjung@kisti.re.kr)

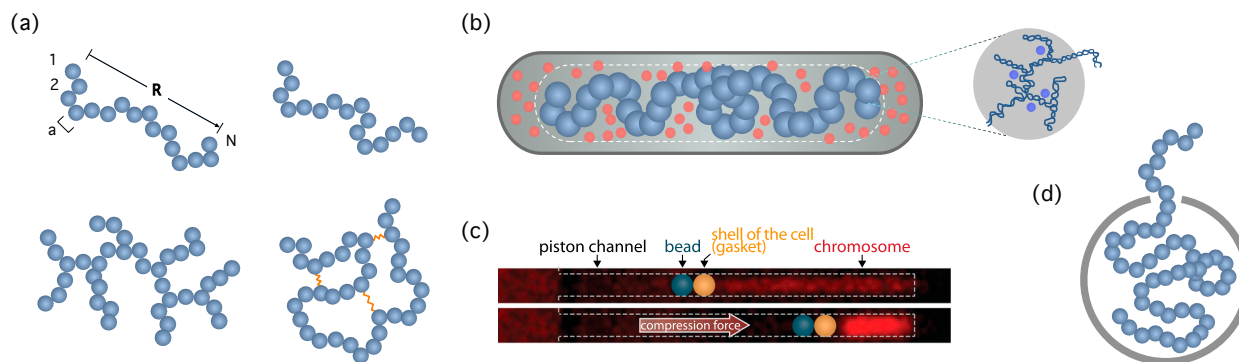


**Fig. 1** (a) Polymers as ‘freedom in chains’<sup>5</sup>: linear polymers (upper) and polymers with a branch-like structure or cross-links (lower). (b) Polymer model of the nucleoid: a model chromosome is packed in part by depletion forces induced by molecular crowding. Each monomer represents the ‘structural unit’ of the bacterial chromosome. (Modified from Ref.<sup>35</sup> by permission of the Royal Society of Chemistry.) (c) Single-molecule manipulations in a confined space, adapted from Ref.<sup>14</sup> (d) Polymer chain release from a confined into free space, reminiscent of the injection of packed viral DNA into a host cell.

similar topics,<sup>13,19,29</sup> it is worth clarifying the scope of this work and its relationship with others. First, the recent review by Reisner et al.<sup>13</sup> is focused on utilizing physical confinement in accessing genetic information encoded in single DNA molecules. In the other reviews,<sup>14,29</sup> some concepts from confined-polymers (e.g., linear ordering and chain segregation, and fractal globules) are used as tools for understanding chromosome organization; if the review by Jun and Wright<sup>14</sup> relies on scaling pictures, especially at the two-chain level, Ref.<sup>29</sup> is focused on single confined chains. In contrast, we place an emphasis on the merits of confined polymers as intriguing physical objects. Also we include new results that have emerged in the last few years; for instance, the role of crowders in organizing chain molecules under confinement has been clarified (see Sec. 3).

While we mainly focus on the equilibrium properties of confined polymers (single or two chains), dynamic quantities such as chain relaxation times can be extracted (see a recent study<sup>13,30</sup> and references therein). Our discussion on polymer chromosome models will be less conclusive. Because of the simplicity of polymers and the complexity of chromosomes, this subfield has evolved more rapidly, in concert with the progress in our understanding of these intricate biological objects.

Other interesting polymer problems include the glassy behavior of polymers<sup>31,32</sup> and the ordering of heteropolymers (e.g., diblock copolymers) into various phases,<sup>33,34</sup> in which confinement has nontrivial effects on their physical (e.g., mobility) or morphological behavior. We believe they deserve separate, more complete discussion, and will not be discussed here.

This review is organized as follows: in Sec. 2, single-chain properties are discussed. Sec. 3 is devoted to chain organiza-

tion by crowding effects, mostly focused on the single-chain case. In Sec. 4, we collect some results for the spatial organization of two chains, especially in a closed confined space. In Sec. 5, we compare a few polymer models of bacterial chromosomes and discuss their implication for chromosome organization and segregation.

Note that unless otherwise stated length scales are measured in units of  $a$  the monomer size, as is particularly the case for simulation results.

## 2 Single-chain case

In this section, we first introduce a few basic concepts such as excluded volume, the Flory exponent, and blobs, primarily as background information for our discussion on confined polymers later in this section. In order to offer a coherent view of confined polymers, we bring together the blob-scaling approach (subsec. 2.2) and Flory theory (subsec. 2.3) as essential theoretical tools and show how they have been reconciled with numerical data. Based on what they offer, we discuss various results regarding single polymer chains (e.g., chain elasticity and confinement free energy), especially under cylindrical confinement. For instance, we present a quantitative basis of (compression) blobs and show how the blob-scaling approach provides a simple physical picture of confined polymers. Flory theory was originally developed as an approximate scheme for calculating the size of linear polymers with excluded volume in an unconfined space. Later in this section, it is extended to such cases as ring polymers and stiff chains, in a cylindrical space. In the course of our discussion, we emphasize how these approaches have benefited each other by offering a complementary picture of single-chain physics under confinement.

## 2.1 Flory exponent and blobs

Consider a polymer chain carrying  $N$  spherical monomers of size  $a$  each in solution (in the absence of confinement). Let  $\mathbf{R}$  be the end-to-end vector of the chain, as shown in Fig. 1(a). The equilibrium size of the chain is often measured by  $\sqrt{\langle \mathbf{R}^2 \rangle}$ . Here and below,  $\langle \dots \rangle$  is an ensemble average. Qualitatively speaking, this is the radius of the chain-explored region, assumed to be overall spherical. In the high-temperature limit or equivalently in an athermal solvent, the excluded volume (the volume taken up by each monomer)  $v \approx a^3$  but it decreases as the temperature is lowered and becomes negative below a certain temperature called the  $\Theta$  temperature. Indeed,  $v$  can be written as  $v \approx a^3(1 - \Theta/T)$ , where  $T$  is the temperature (see for instance Refs.<sup>2,3</sup>).

The chain is swollen by the excluded-volume interaction between monomers and is often referred to as a self-avoiding chain. A perturbative approach, in which the excluded volume interaction is treated as a perturbation, leads to<sup>3</sup>

$$\langle \mathbf{R}^2 \rangle = R_0^2 \left( 1 + \frac{4}{3}z - 2.075z^2 + \dots \right), \quad (1)$$

where  $R_0 = a\sqrt{N}$  is the ideal-chain size ( $v = 0$ ) and  $z$  is the expansion or chain interaction parameter given by<sup>2,3</sup>

$$z = \left( \frac{3}{2\pi} \right)^{3/2} \frac{v}{a^3} \sqrt{N}. \quad (2)$$

When  $v = a^3$ , the series in Eq. 1 diverges even for small  $N$ . This means that the effect of self-avoidance is significant for any realistic  $N$  value, more so for larger  $N$ , or at any length scale somewhat beyond  $a$ . For  $v/a^3 < 1$ , however, self-avoidance is significant for  $N$  larger than a certain value, denoted as  $g_T$ . The corresponding length scale is known as the thermal blob size  $\xi_T = a\sqrt{g_T}$ .<sup>1,2</sup> By setting the second term in Eq. 1 with  $N = g_T$  to unity, we find  $\sqrt{g_T} \approx a^3/v$  and  $\xi_T \approx a^4/v$ .<sup>1,2</sup>

The perturbation expansion is, however, not useful for calculating the size of an excluded-volume chain. Flory theory is a much celebrated theoretical scheme for calculating the chain size or the Flory radius  $R_F$  (see also Subsec. 2.3), which produces<sup>1,2</sup>

$$R_F = \sqrt{\langle \mathbf{R}^2 \rangle} \approx \xi_T \left( \frac{N}{g_T} \right)^{\nu} \approx a \left( \frac{v}{a^3} \right)^{2\nu-1} N^{\nu} \xrightarrow{v=a^3} aN^{\nu}, \quad (3)$$

where the Flory exponent  $\nu = 3/5$  (in three dimensions) is larger than  $1/2$  expected for an ideal or random walk chain. \* Unless otherwise stated, for simplicity, we mainly focus our consideration on the athermal case  $v \approx a^3$  or stiff chains.

\* The Flory exponent is close to a more accurate value of  $\nu \approx 0.588$  (see Ref.<sup>3</sup> and relevant references therein).

A related quantity is the free energy of a self-avoiding chain with the two ends held at  $R = |\mathbf{R}|$ , which assumes the following scaling form

$$\mathcal{F}(R) \approx k_B T \left( \frac{R}{R_F} \right)^{\delta}, \quad (4)$$

where  $\delta = 2$  for  $R < R_F$  and  $\delta = 5/2$  for  $R > R_F$ .<sup>1-3</sup> As a result, a self-avoiding chain responds to an external force  $f$  as<sup>1,2,36</sup>

$$f = \frac{\partial \mathcal{F}(R)}{\partial R} \approx \left( \frac{k_B T}{R_F} \right) \left( \frac{R}{R_F} \right)^{\delta-1}. \quad (5)$$

Here  $R$  should be understood as a new equilibrium chain size under  $f$  along the force direction ( $R_f$  is often used for this quantity<sup>1,2</sup>).

Note that a single exponent cannot characterize  $F(R)$  fully. For  $R < R_F$ , the exponent  $\delta = 2$  is well aligned with our expectation that the chain behaves as a Hookean spring for small deformations with an effective spring constant  $k_{\text{chain}} \approx k_B T/R_F^2$ . For large  $f$ , corresponding to  $R > R_F$ , the force-extension relation is non-linear:  $f \approx (k_B T/R_F)(R/R_F)^{3/2}$ .<sup>1,36</sup>

Our discussion below relies much on the notion of blobs.<sup>1,2,36</sup> (Thermal blobs are simple examples of blobs.) It is thus instructive to offer a blob picture of the result in Eq. 4, especially in the large- $R$  limit. (See Refs.<sup>1,2,36</sup> for more details.) Imagine stretching a self-avoiding chain with an external force  $f$ , as shown in Fig. 2(d). The force tends to align the chain along the force direction. This tendency is, however, opposed by chain entropy, which favors coiled conformations. As a result, the force effect will be felt only beyond a length scale  $\xi$ , the tensile-blob size. The chain can then be viewed as a linear string of (tensile) blobs, each consisting of  $g$  monomers:  $R \approx (N/g)\xi$ , where  $\xi \approx ag^{\nu}$  (athermal). Since each blob stores an excess free energy of  $k_B T$ ,<sup>†</sup> one can establish

$$\frac{\mathcal{F}(R)}{k_B T} \approx \frac{N}{g} \approx \frac{R}{\xi} \approx \left( \frac{R}{R_F} \right)^{5/2}, \quad (6)$$

where we eliminated  $g$  and  $N$  in favor of  $R$  and  $R_F$  via  $R \approx (N/g)\xi$  and  $R_F \approx aN^{\nu}$ , respectively, in the final step. This is identical to the large- $R$  result in Eq. 4 and is thus consistent with the non-linear force-extension relation. It also offers a free-energy picture of a blob: a free-energy cost of  $k_B T$  per blob for stretching a self-avoiding chain.

It is straightforward to show  $\xi f \approx k_B T$  or  $\xi \approx k_B T/f$  from Eq. 6.<sup>‡</sup> In other words, the work required for aligning a blob along the force direction is comparable to  $k_B T$ , consistent with

† Thermal blobs can be interpreted similarly:  $\xi_T$  is a length scale at which the (excess) excluded volume interaction becomes comparable to  $k_B T$ , as detailed in subsec. 2.3.

‡ This can be rewritten as  $f \approx (k_B T/\xi^2)\xi$ . It is a special case of the small  $R$  result in Eq. 4 for  $R = R_F = \xi$ .

our view of blobs: inside each, the effect of  $f$  is not felt appreciably.

Under cylindrical confinement, a self-avoiding chain will experience a similar alignment along the long symmetry axis of the cylinder. The stretched and cylindrically-confined cases can map onto each other through  $D \approx \xi \approx k_B T / f$ .<sup>1,6</sup> Various quantities can be obtained within the blob picture, as detailed below.

## 2.2 Blob-scaling theory and numerical data

It is hard to overstate the impact on polymer physics of the blob-scaling approach pioneered by de Gennes.<sup>1</sup> It allows us to visualize how internal interactions or external perturbations influence chain statistics and conformations; subsec. 2.1 only catches a glimpse of this. In this picture, a chain is viewed as a string of blobs (see Ref.<sup>37</sup> for a quantitative picture of blobs); within each blob, chain statistics is assumed to be unaltered by internal or external perturbations: the influence of other segments on the same chain (internal) or that of other chains, confinement, or external forces (external). This simple picture has proven to be useful for understanding various polymeric systems: semidilute polymer solutions<sup>1,2</sup> and electrically-charged<sup>38–40</sup> or confined polymers.<sup>1,2,6,41–43</sup> It enables one to obtain scaling results for reptation and chain relaxation times.<sup>1,2</sup> The blob scaling approach has recently been extended to study how two chain molecules are spatially organized in an open cylinder<sup>44</sup> or closed two-dimensional box.<sup>45</sup>

**2.2.1 Flexible chains**—If trapped in an open cylindrical space, a polymer chain breaks up into a linear string of (compression) blobs, as illustrated in Fig. 2(a)–(c).<sup>1,2</sup> Let  $N$  be the number of monomers,  $D$  the diameter of the cylinder,  $\xi$  the blob size ( $\xi \approx D$ ), and  $g$  the number of monomers per blob. One can then establish  $g \approx (D/a)^{1/\nu}$ , where  $\nu = 3/5$  is the Flory exponent.<sup>1,2,6,7</sup> This leads to the equilibrium chain size

$$L_0 = \langle X \rangle \approx \left( \frac{N}{g} \right) \xi \approx Na \left( \frac{D}{a} \right)^{1-1/\nu} \approx Na \left( \frac{D}{a} \right)^{-2/3}. \quad (7)$$

Here and below,  $X$  is the longitudinal size of a confined chain; recall  $\langle \dots \rangle$  is an assemble average.

By assigning  $k_B T$  to each blob, the confinement-free energy can be obtained as<sup>1,2,6,7</sup>

$$\frac{\mathcal{F}_{\text{conf}}}{k_B T} \approx \frac{N}{g} \approx N \left( \frac{D}{a} \right)^{-1/\nu} \approx N \left( \frac{D}{a} \right)^{-5/3}. \quad (8)$$

If we consider the chain as a series connection of independent blobs with a spring constant  $k_{\text{blob}} \sim k_B T / D^2$  each,<sup>§</sup> we arrive

§ This can be readily obtained from Eq. 4 with  $\delta = 2$ . Alternatively, the weak blob-deformation free energy can be written as  $\mathcal{F}_{\text{blob}}/k_B T \approx (u_{j+1} - u_j)^2 / 2\xi^2$ , where  $\xi \approx D$  and  $u_j$  is the position of the  $j$ -th blob.<sup>6</sup> Let  $\delta\xi$  describe the blob-size deformation. Then this free energy implies  $\mathcal{F}_{\text{blob}}/k_B T \approx (\delta\xi)^2 / 2\xi^2$ , resulting in  $k_{\text{blob}} = k_B T / \xi^2$ .

at the spring constant of the chain given by<sup>30,46,47</sup>

$$\frac{k_{\text{chain}}}{k_B T} \approx \frac{1}{(N/g)D^2} \approx N^{-1} D^{-1/3} a^{-5/3}. \quad (9)$$

Linear ordering induced by cylindrical confinement has a direct consequence on the way two chains interact and segregate. If mixed and arranged in parallel with each other in a cylindrical space (with open ends), each chain can be viewed as trapped in an imaginary cylinder with a reduced diameter  $D_{\text{eff}} \approx D/\sqrt{2}$ .<sup>21</sup> This enables us to calculate the free energy of a mixed state:

$$\mathcal{F}_{\text{mix}} = 2^{1/2\nu} \mathcal{F}_{\text{seg}} > \mathcal{F}_{\text{seg}}, \quad (10)$$

where  $\mathcal{F}_{\text{seg}}$  is the free energy of a segregated state given by  $\mathcal{F}_{\text{seg}} = 2\mathcal{F}_{\text{conf}}$ , where  $\mathcal{F}_{\text{conf}}$  is the confinement free energy of each chain given in Eq. 8. This means that chain mixing is disfavored by free energy.

Similarly, a polymer in a spherical cavity of diameter  $D$  can be considered as being made of blobs (see Fig. 2(e)). The main difference is that there is no *directionality* in this case, in contrast to the cylindrical case, in which the long symmetry axis of the cylinder naturally serves as the director. In a self-avoiding walk analogy, there is no preferred directionality for the walker in a spherical space. Thus, the confined polymer is a random packing of blobs of size  $\xi$ , given by

$$\xi \approx a (D^3/a^3 N)^{\frac{\nu}{3\nu-1}} \approx a\phi^{-\frac{\nu}{3\nu-1}} \approx a\phi^{-3/4}, \quad (11)$$

where  $\phi$  is the volume fraction of monomers. The confinement-free energy can be obtained by assigning  $k_B T$  to each blob<sup>41,48</sup>:

$$\frac{\mathcal{F}_{\text{conf}}}{k_B T} \approx \frac{D^3}{\xi^3} \approx \left( \frac{D^3}{a^3} \right) \phi^{\frac{3\nu}{3\nu-1}} \approx N\phi^{\frac{1}{3\nu-1}} \approx N\phi^{-5/4}. \quad (12)$$

Note that the final expression is linear with  $N$  for a fixed  $\phi$ . If  $N$  doubles while  $\phi$  or  $\xi$  remains fixed,  $\mathcal{F}_{\text{conf}}$  also doubles, similar to what we would expect from the cylindrical case. In the latter case,

$$\frac{\mathcal{F}_{\text{conf}}}{k_B T} \approx N \left( \frac{D}{a} \right)^{-1/\nu} \approx N \left( \frac{\xi}{a} \right)^{-1/\nu} \approx N\phi^{\frac{1}{3\nu-1}} \approx N\phi^{-5/4}. \quad (13)$$

The scaling form of  $\mathcal{F}_{\text{conf}}$  for spherical confinement (or simply  $\mathcal{F}_{\text{sphere}}$ ) was confirmed numerically.<sup>41,42</sup> For  $\phi < 0.15$ , the blob-scaling picture remains valid (assuming  $R_F > D$ ), as also shown in Fig. 2(f). For  $\phi > 0.15$  (in the yellow region in the graph), however, the blob picture breaks down. In this regime, three-body terms contribute appreciably to  $\mathcal{F}_{\text{sphere}}$ . This explains why the free energy curve is steeper in this regime.

The analogy between the spherically and cylindrically confined cases seems obvious since in both cases  $k_B T$  is assigned

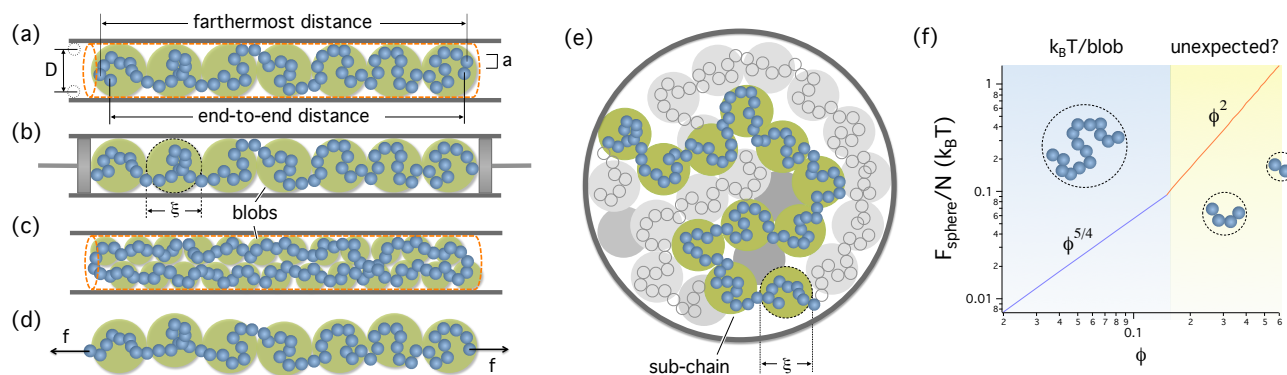


**Fig. 2** Confined or constrained flexible polymers with self-avoidance (adapted from Ref. <sup>37</sup> by permission of the Royal Society of Chemistry). (a)-(c) Cylindrically-confined polymers. The diameter  $D$  is defined in (a) so that  $D \rightarrow 0$  the confined chain becomes “perfectly” linearly organized, in parallel with the continuum analogue. (a) As a measure of the chain size  $L$ , one can use the end-to-end distance, the farthest distance, or the length of a tube (red-dashed) occupied by the chain; the latter two can be used interchangeably. In (b), the piston-piston distance naturally defines the chain size. (c) For a ring polymer, the farthest distance or the tube length can be chosen as the chain size. (d) A stretched chain with an external force  $f$  maps onto the chain in (a)-(b), if  $D \approx k_B T / f$  is chosen (as long as  $D$  is somewhat larger than  $10a$  or if each blob is “well-defined”<sup>37</sup>).<sup>1,2</sup> (e) A spherically-confined chain can be viewed as being made of several ‘subchains’<sup>41</sup>; a subchain is a section of the confined chain from somewhere on the wall to elsewhere on the wall, inside which the direct wall effect is not felt. It can map onto an equivalent semi-dilute solution, the cylindrically-confined (b) or stretched chain in (d). In all these cases, the free energy cost for perturbing the chains by confinement,  $f$ , or other sub-chains is  $k_B T$  per blob (if each blob is well defined). The graph in (f), partly based on the blob picture, shows how the free energy for case (e) varies as a function of the monomer volume fraction  $\phi$  [Reprinted (adapted) with permission from Ref. <sup>42</sup> Copyright (2006) American Chemical Society.] This analogy between (a), (b) (d) and (e) helps us understand when the  $k_B T$ -per-blob picture breaks down and why the non-blob scaling regime emerges.<sup>37</sup>

to each blob. However, it appears to deviate from the more conventional view that the confinement free energy increases more rapidly in the spherical case if plotted against the degree of confinement  $R_F/D$  (recall  $R_F \approx aN^{\nu}$  is the Flory radius).<sup>42</sup> As pointed out in Ref.,<sup>37</sup> however, this is a seeming difference. As  $D$  decreases,  $\phi$  increases more rapidly in the spherical case; as a result, the confinement free energy increases more rapidly. But for a given  $\phi$ , the free energy is linear in both cases.

On the other hand, the analogy between a polymer under cylindrical confinement and a polymer under tension has long been appreciated<sup>1,6</sup> (see Fig. 2(d)). As discussed earlier, the two cases map onto each other through  $\xi \approx D \approx k_B T / f$  or  $f \approx k_B T / \xi \approx k_{\text{blob}} \xi$  (recall  $k_{\text{blob}} \approx k_B T / \xi^2$ ). This relation, describing a Hookean response of a blob, holds for both ideal and self-avoiding chains. Under this condition, the work required to align a blob along the direction of  $f$  becomes  $W = f\xi \approx k_B T$ , i.e., comparable to  $k_B T$ ; inside a blob, the effect of  $f$  is a small perturbation.

Despite its much appreciation, however, the blob scaling approach has only recently been tested against numerical and theoretical results. For instance, a theoretical approach, known as a uniform expansion method,<sup>3</sup> confirmed the scaling relation in Eq. 7.<sup>49</sup> On the other hand, Fig. 3 summarizes some of recent numerical results<sup>37</sup>: (a) the internal distance

$R_{ij} = \sqrt{\langle \mathbf{R}^2(|i-j|) \rangle}$  defined as the average distance between monomers at  $i$  and  $j$ , (b)  $L_0 = \langle X \rangle$  as a function of  $D$ , and (c) the variance of the chain size  $\sigma_L^2$  (per monomer) vs.  $D$ . The results in (a) offer a quantitative basis of blobs: self-avoiding walk within  $\xi \approx D$  and linear ordering beyond  $\xi$ . The graph in (b) confirms the scaling relation in Eq. 7. It also suggests that the farthest distance is a better choice as the chain size than the end-to-end distance, in the sense that the former (filled symbols) follows the blob-scaling picture (the dashed line) in a wider parameter range.<sup>37</sup>

The results in (c) clarify the applicability of Eq. 9 (see (c)).<sup>37</sup> In this connection, it is worth mentioning that the blob scaling limit is more readily reached for  $L_0$  than for  $k_{\text{chain}}$ .<sup>37,46</sup> The variance  $\sigma_L^2$  is related to  $k_{\text{chain}}$  as  $k_{\text{chain}} = k_B T / \sigma_L^2$ . (The right axis is the relaxation time given by  $\tau \sim \sigma_L^2 / N$ , measured in the absence of hydrodynamic interactions<sup>37</sup>; it is thus directly related to  $\sigma_L^2 / N$ .) For small  $D$ , the results in Fig. 3(c) deviate from the blob scaling picture, which predicts a slope  $1/3$  in this log-log plot. The crossover at  $D \approx 10$  (in units of  $a$ ) from the blob-scaling to formally-called unexpected regime (characterized by a large slope 0.9)<sup>30,46,47</sup> can be attributed to the “fate” of blobs for small  $D$ .<sup>¶</sup> As discussed earlier in

¶ [Note that the slope of a fitting curve for the small  $D$  range may depend somewhat on simulation details or fitting methods. For instance, refer to Fig. 2(a) for the definition of  $D$ . Also it is worth noting that a few data points for  $D < 2$  deviate slightly from and fall below the fitting curve (dashed line). As a result,

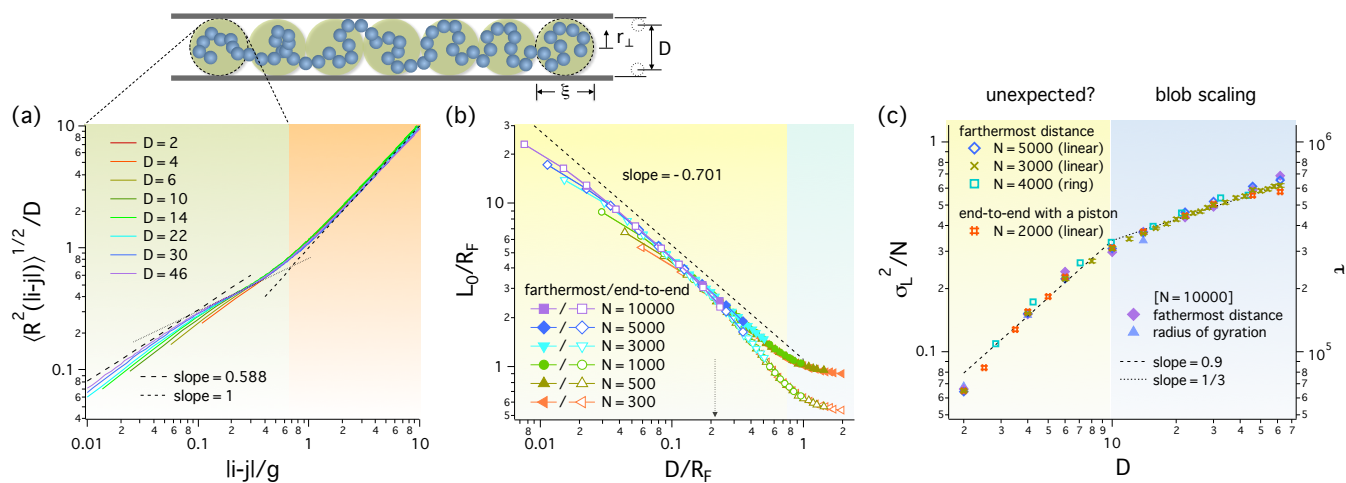


**Fig. 3** Blobs, linear ordering, and chain elasticity (adapted from Ref.<sup>37</sup> by permission of the Royal Society of Chemistry). (a) The simulation results for the internal distance  $R_{ij} = \sqrt{\langle R^2(|i-j|) \rangle}$  in (a) show how the confined chain is organized: it resembles a self-avoiding chain within each blob of size  $\xi \approx 0.7D$  and is linearly ordered beyond  $\xi$ , the blob size. This offers a quantitative basis of compression blobs.<sup>1,6</sup> (b) The farthest distance (filled symbols) follows the blob-scaling picture (the dashed line) in a wider parameter range than the end-to-end distance (unfilled symbols) does, since this quantity is less sensitive to chain-end effects. As  $D \rightarrow 0$ , the difference between the two sets of data (filled and unfilled) becomes insignificant but they deviate somewhat from the simple power-law relation. (c) The variance of the chain size  $\sigma_L^2$  is displayed against  $D$ ;  $\sigma_L^2$  is related to the (effective) chain spring constant as  $k_{\text{chain}} = k_B T / \sigma_L^2$ . (The right axis is the relaxation time given by  $\tau \sim \sigma_L^2 / N$ , measured in an imaginary immobile solvent or in the absence of hydrodynamic interactions<sup>37</sup>; it is thus directly related to  $\sigma_L^2 / N$ .) The blob picture predicts a single slope 1/3 in this log-log plot. It, however, breaks down as  $D \rightarrow 0$ . This explains the crossover at  $D \approx 10$  (in units of  $a$ ) from the blob-scaling to formally-called unexpected behavior (with a slope 0.9). It was noted that this crossover can be best understood by drawing an analogy between this case and the corresponding spherically confined case.<sup>37</sup>

correction with  $\mathcal{F}_{\text{sphere}}$  in Fig. 2(f), the notion of blobs becomes less meaningful as they become sufficiently small. It was noted that this crossover can be best understood by drawing an analogy between this case and the corresponding spherically confined case.<sup>37</sup>

Indeed it was also shown that the blob scaling results for chain elasticity are applicable when these two conditions are simultaneously met: the blob size should exceed  $10a$  and  $N > N_{\text{min}}$ .<sup>37</sup> Intriguingly,  $N_{\text{min}}$  depends on how the chain size is measured (see Fig. 2(a) for the end-to-end distance, the farthest distance, and the length of a tube enclosing the chain are depicted):  $N_{\text{min}} \approx 1000$ , if the farthest distance is used as the chain size (as in Fig. 3(c)). As a result,  $\sigma_L^2$  becomes less sensitive to chain-end effects. These unfavorable effects can be “corrected” in a micro-nano-piston experiment, where the two chain ends are attached to the piston wall (see Fig. 2(b)). Also the farthest distance is relevant for ring polymers with no ends as shown in Fig. 2(c) (e.g., bacterial chromosomes). The radius of gyration is expected to be less sensitive to chain-end effects and will be a convenient choice for polymers with non-linear topology (e.g., branched or ring polymers).<sup>37</sup> The chain-end effect is significant, if the end-to-end distance is used as the chain size, and as a result  $N_{\text{min}} \approx 12000$ . Even in the limit  $N \rightarrow \infty$ , however, the blob scaling regime for  $k_{\text{eff}}$  will not be reached for  $D < 10a$ .<sup>37</sup>

A similar discrepancy was seen and resolved in the problem of a self-avoiding chain subject to an external force  $f$ .<sup>36</sup> According to the blob picture,<sup>1,36</sup> the chain extension along  $f$  varies nonlinearly as  $f^{2/3}$ . This scaling relation was not observed in a numerical study with  $N = 1600$ .<sup>50</sup> More recently, however, experiments with single stranded DNA (10.5 kilobase pair long) verified the existence of this regime.<sup>51</sup> Considering the analogy between the stretched and cylindrically-confined cases, it will be useful to simulate a longer chain so that it contains many well-defined ‘tensile’ blobs.<sup>1,36</sup>

**2.2.2 Semiflexible chains or flexible chains with weak self-avoidance**—So far, we have focused on flexible chains consisting of beads modelled as hard spheres with the excluded volume given by  $v \approx a^3$ . Recall that this is relevant in an athermal solvent. The conformation of such a chain resembles the trajectory of a self-avoiding walk with a step length  $a$ . Under different conditions, the strength of self-avoidance can be weaker. For instance, as the temperature is lowered, the excluded-volume interaction between monomers is diminished (and can even be attractive).<sup>1–3</sup> (see Ref.<sup>52</sup> for chain collapse at a low temperature). Chain stiffness gives rise to similar effects. As a result, a new length scale enters into our consideration: the size of a thermal blob  $\xi_T$ , within which self-avoidance is not felt, as illustrated in Fig. 4. As discussed

in subsec. 2.1, for spherical monomers,  $\xi_T \approx a^4/v \propto a$ .<sup>1,2</sup> (For cylindrical monomers of length  $b$  and width  $w$  each in an thermal solvent,  $v \approx b^2w$  and  $\xi_T \approx b^4/v \approx b^2/w$  (see subsec. 2.3.3 and Ref.<sup>2</sup>)) How will this influence chain statistics and elasticity?

Fig. 4 shows how the crossover between different regimes occurs as  $D$  decreases. For  $D \gg \xi_T$  (see Fig. 4(a)), the confined chain can still be viewed as a linear array of approximately spherical blobs of size  $\xi$  each, as assumed in the blob approach<sup>1</sup>; as it turns out  $\xi \approx 0.7D$  for spherical monomers in an athermal solvent.<sup>37</sup> Also the scaling relations presented in subsec. 2.2.1 remain relevant in the sense that the  $N$ - $D$  dependence of  $L_0$ ,  $\mathcal{F}_{\text{conf}}$ , and  $k_{\text{chain}}$  remains unaltered. (See the Flory radius in Eq. 3 for an unconfined analogue; the scaling form of the Flory radius remains invariant.)

In contrast, these blobs will be elongated along the long axis of the cylinder, if  $D > \xi_T$  is not satisfied – weakening of self-avoidance delays the emergence of the linear regime, as illustrated in Fig. 4(b). In this case, the confined chain can be viewed as a linear array of elongated blobs of size  $\xi_{\parallel}$  each ( $\xi_{\parallel} > D$ ). The corresponding regime is often referred as the ‘extended de Gennes’ regime.<sup>13,15–17</sup>

The elongated-blob picture does not modify the scaling form of  $L_0$ ; up to a numerical prefactor,  $L_0$  is the same in the de Gennes and extended de Gennes regimes.<sup>15–17</sup> Obviously,  $L_0 \sim N$ , since the chain is linearly ordered beyond  $\xi_{\parallel}$ . The  $D$ -dependence is less obvious but can be obtained using single physical arguments (see subsec. 2.3.3). In contrast, the confinement free energy can be approximated as  $\mathcal{F}_{\text{conf}} \sim N(D/a)^{-2}k_B T$ , which has the same scaling form as the confinement free energy of a corresponding ideal chain<sup>1</sup> (see Ref.<sup>16</sup> and relevant discussions below). In other words, self-avoidance is not reflected well in  $\mathcal{F}_{\text{conf}}$ . This can be understood as follows: for  $D \ll \xi_T$ , the elongated blobs do not serve as free-energy “currency” (i.e.,  $k_B T/\text{blob}$ ). In a self-avoiding walk (SAW) analogy, there will be a free energy cost each time the “weak” SAW changes its direction upon colliding into the cylindrical wall or each time it travels a distance comparable to  $D$  in the transverse distance. On the other hand, within this distance, it behaves as a random walk (RW). This explains why self-avoidance is not reflected in the confinement free energy in the extended de Gennes regime. (As it turns out, the effect of self-avoidance is subdominant, as detailed in the next section.)

As  $D$  decreases further, a new regime known as the Odijk regime emerges (see Fig. 4(c)). This regime is more meaningful for stiff chains for which the persistence length  $\ell_p$  can be much larger than  $D$ , as originally assumed.<sup>53–55</sup> In this case, a new length scale known as the deflection length  $\lambda_{\text{def}}$  becomes relevant, which is given by  $\lambda_{\text{def}}^3 \approx D^2 \ell_p$ . This is a length scale within which the stiff chain does not feel cylindrical confinement. The confinement free energy of a long

the slope will depend on whether these points are included; if more of such data points were included, the slope would be somewhat larger.

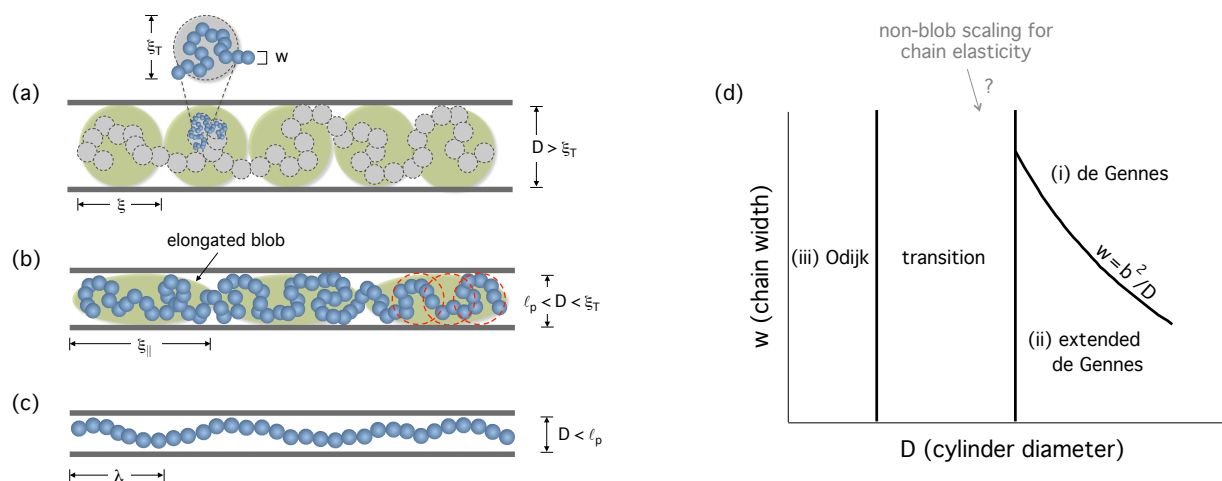


**Fig. 4** Organization of polymers with weak self-avoidance in a cylindrical space characterized by a few regimes [adapted (with modifications) with permission from Ref. <sup>16</sup> Copyright (2014) American Chemical Society]. Weak self-avoidance can result from a temperature decrease or chain stiffening, often measured by the persistence length  $\ell_p$ . In this case, a new length scale, i.e., the thermal blob size  $\xi_T$ , enters into the picture. Inside each blob or within  $\xi_T$ , self-avoidance is not felt. (a) de Gennes regime: for  $D \gg \xi_T$ , our blob-scaling picture remains relevant:  $L_0 \sim ND^{1-1/\nu}$  and  $\mathcal{F}_{\text{conf}} \sim ND^{-1/\nu}$ . (b) Extended de Gennes regime: for  $\ell_p \ll D \ll \xi_T$ ,  $L_0 \sim ND^{1-1/\nu}$  as in (a) and  $\mathcal{F}_{\text{conf}} \sim ND^{-2}$  as for an ideal chain. In this case, the chain can be viewed as a linear succession of elongated blobs of size  $\xi_{\parallel}$  each, beyond which the chain is linearly organized. Also shown are red circles of size  $D$  each as free-energy units: within each circle, cylindrical confinement is not felt. Each time the self-avoiding chain travels a distance  $D$ , there is an associated free energy cost for confinement. For  $D \ll \xi_{\parallel}$ ,  $\mathcal{F}_{\text{conf}}$  should resemble the one for the corresponding ideal chain. (In the transition regime, the confined chain contains isolated ‘hairpin backbends.’<sup>13</sup>) (c) Odijk regime: when  $D \ll \ell_p$ , the confined chain enters the Odijk regime, in which the reflection length  $\lambda_{\text{def}}$  describes the degree of confinement; within this length, the confined chain does not feel the effect of confinement. This regime is realized for a locally stiff chain for which  $\ell_p \gg a$ . The diagram in (d) depicts the regimes in (a)-(c) and their boundary.

chain ( $L_{\text{total}} > \ell_p$ ) is expressed as  $\mathcal{F}_{\text{conf}}/k_B T \approx L_{\text{total}}/\lambda_{\text{def}}$ , if  $\ell_p \gg \lambda_{\text{def}}$  or  $\ell_p \gg D$ ,<sup>53–55</sup> where  $L_{\text{total}}$  is the total contour length (also see Ref.<sup>56</sup> for the numerical prefactor of  $\mathcal{F}_{\text{conf}}$ ).

How does the non-blob scaling regime in Fig. 3(c) fit into the diagram in Fig. 4(d)? For a flexible chain in an athermal solvent, this regime will fall somewhere in the transition regime. For a more complete picture, it will be useful to extend earlier studies of chain elasticity under confinement<sup>30,37,46,47</sup> to the extended de Gennes regime. As noted earlier,<sup>37,46</sup> the scaling regimes describing chain sizes are not necessarily identical to those describing chain elasticity/relaxation. One possibility is to manipulate a confined chain with an external force, as shown in Fig. 2(b) with varying  $\ell_p$  and  $D$ .

### 2.3 Flory theory

Flory theory is a brilliant scheme for calculating the size of a self-avoiding chain. Despite its potential limitations as a meanfield model, because of its simplicity, the Flory approach has been widely employed in the literature and extended to confined polymers.<sup>13,16,21,30,37,47,57</sup> Here we briefly recapture earlier discussions on the Flory approach and highlight how this approach has evolved and been reconciled with other approaches.

**2.3.1 Linear chains**—Consider a flexible polymer carrying  $N$  monomers in an athermal solvent, with  $R$  being its end-to-end distance. The Flory free energy in  $d$ -spatial dimensions is then expressed as

$$\frac{\mathcal{F}_{\text{Flory}}(R)}{k_B T} \approx \frac{R^2}{Na^2} + \frac{a^d N^2}{R^d}, \quad (14)$$

If the first term describes chain elasticity, the second term represents the two-body interaction between monomers along the chain.<sup>1,58</sup> The free energy  $\mathcal{F}_{\text{Flory}}$  is minimized at  $R = R_F$ : for  $d \leq 4$ ,  $R_F \approx aN^\nu$ , where  $\nu$  is the Flory exponent, given by  $\nu = 3/(2+d)$  (e.g.,  $\nu = 3/5$  for  $d = 3$ ).

Flory theory produces a correct  $R_F$ , but as noted in Ref.,<sup>1</sup> this success benefits from a ‘remarkable cancellation’ of errors. Indeed,  $\mathcal{F}_{\text{Flory}}$  in Eq. 14 implies that the chain spring constant for  $d = 3$  is given by

$$k_{\text{chain}} \approx \left( \frac{\partial^2 \mathcal{F}_{\text{Flory}}}{\partial R^2} \right)_{R=R_F} \approx \frac{k_B T}{Na^2}. \quad (15)$$

This is an overestimate in view of the correct one discussed earlier in subsec. 2.1 and in the literature<sup>1</sup>

$$k_{\text{chain}} \approx \frac{k_B T}{R_F^2} \approx \frac{k_B T}{N^{6/5} a^2}. \quad (16)$$

See Refs.<sup>59,60</sup> for a rigorous treatment of the limitation of Flory theory.

For a polymer under cylindrical confinement, however, it was shown that a ‘correct’ (renormalized) Flory approach<sup>||</sup> can be constructed.<sup>30,47</sup> Let  $X$  be the chain size in the longitudinal direction, then the Flory free energy can be expressed as

$$\frac{\mathcal{F}_{\text{cyl}}(X, D)}{k_B T} \approx \frac{X^2}{(N/g)D^2} + \frac{D(N/g)^2}{X}, \quad (17)$$

where  $g$  is the number of monomers inside a blob of diameter  $D$  introduced earlier, i.e.,  $g \approx (D/a)^{5/3}$ . This free energy describes an imaginary chain consisting of  $N/g$  subunits (blobs) of size  $D$  in an one-dimensional space. In other words, blobs are considered as the subunits of the chain. Note that this approach remains valid unless the chain is much compressed longitudinally (assuming  $D > 10a$ ).<sup>47</sup>

Indeed, the free energy in Eq. 17 produces not only the expected equilibrium chain size  $L_0 \equiv \langle X \rangle \approx Na(a/D)^{2/3}$ , at which  $\mathcal{F}_{\text{cyl}}(X, D)$  is minimized, but also the correct confinement free energy<sup>1,6</sup>:

$$\frac{\mathcal{F}_{\text{conf}}}{k_B T} = \frac{\mathcal{F}_{\text{cyl}}(X = L_0)}{k_B T} \approx \frac{N}{g} \approx N \left( \frac{a}{D} \right)^{5/3}. \quad (18)$$

It also leads to the correct effective spring constant of the chain<sup>6,61</sup>:

$$k_{\text{chain}} = \left( \frac{\partial^2 \mathcal{F}_{\text{cyl}}}{\partial X^2} \right)_{X=L_0} \approx \frac{1}{Na^2} \left( \frac{a}{D} \right)^{1/3} k_B T. \quad (19)$$

A natural extension of Eq. 17 is the free energy of a chain confined in a slit geometry<sup>2</sup>, i.e., two parallel plates separated by a distance  $D$ . If  $R_{\parallel}$  is the chain size in the direction parallel with the slit, the slit free energy is given by

$$\frac{\mathcal{F}_{\text{slit}}(R_{\parallel}, D)}{k_B T} \approx \frac{R_{\parallel}^2}{(N/g)D^2} + \frac{D^2(N/g)^2}{R_{\parallel}^2}, \quad (20)$$

where  $g \approx (D/a)^{5/3}$  is the same as in a cylindrical space.<sup>2</sup> Indeed, this free energy reproduces the correct equilibrium size of the chain in a slit,  $L_0 \approx N^{3/4} a(a/D)^{1/4}$ .<sup>2,57</sup> However, its equilibrium free energy,  $\mathcal{F}_{\text{slit}}(X = L_0, D)/k_B T$ , scales as  $N^{1/2}(a/D)^{5/3}$ . Note that this is different from the expected free energy of slit confinement  $\mathcal{F}_{\text{conf}}/k_B T \approx N/g \approx N(a/D)^{5/3}$ , which is identical to that of a cylindrically confined polymer (see Refs.<sup>1,2</sup> and references therein). At best, the slit free energy in Eq. 20 describes the interaction of blobs in a slit at the meanfield level (possibly overestimated), not confinement.

In summary, the cylindrical case is a special one in that the excluded-volume interactions between blobs separated by a long-contour distance are not allowed. The conformational deformation of the confined chain resembles that of a

<sup>||</sup> It is correct in the sense that it remains valid in the Hookean limit or when  $X \approx L_0$ .<sup>47</sup>

(quasi one-dimensional) Rouse chain formed by renormalized monomers of size  $\xi \approx D$  each.<sup>6</sup> The corresponding renormalized Flory approach does not suffer from overestimate errors.

**2.3.2 Ring polymers**—Earlier studies suggest that a ring chain maps onto a parallel connection of two linear chains, each consisting of  $N/2$  monomers trapped in an imaginary tube of a reduced diameter  $D_{\text{eff}} \approx D/\sqrt{2}$ .<sup>21</sup> Note that this was originally established for rather small  $D$  values but is expected to remain relevant for larger  $D$  on physics grounds. This mapping allows one to extend the renormalized Flory approach in Eq. 17 to ring polymers. To this end, let us rewrite Eq. 17 as

$$\frac{\mathcal{F}_{\text{linear}}(X)}{k_B T} = A \frac{X^2}{(N/g)D^2} + B \frac{D(N/g)^2}{X}, \quad (21)$$

where  $A$  and  $B$  are (non-universal) constants of order 1. We then adjust  $N$  and  $D$  so that they represent one of the two linear chains. This line of reasoning leads to

$$\frac{\mathcal{F}_{\text{ring}}(X)}{k_B T} \approx \hat{A} \frac{X^2}{(N/g)D^2} + \hat{B} \frac{D(N/g)^2}{X}, \quad (22)$$

where  $\hat{A} = 2^{13/6}A$  and  $\hat{B} = 2^{1/6}B$ . Note here that the parameters  $g, N$ , and  $D$  on the right hand side are for the corresponding linear chain case. The effect of ring topology is absorbed into  $\hat{A}$  and  $\hat{B}$ .

The equilibrium size is then given by  $L_{\text{ring}} \approx 0.630 \times L_{\text{linear}}$ , where  $L_{\text{linear}} = (B/2A)^{1/3}D(N/g)$  is the equilibrium chain size for the corresponding linear case. The confinement free energy then reads  $\mathcal{F}_{\text{ring}}(L_{\text{ring}}) \approx 2^{5/6} \times \mathcal{F}_{\text{linear}}(L_{\text{linear}})$ . Furthermore,  $k_{\text{ring}} \approx 2^{13/6}k_{\text{linear}}$  or  $k_{\text{ring}}/k_{\text{linear}} \approx 4.5$ . Ring topology stiffens a confined chain about 4.5 fold. See Ref.<sup>21</sup> for a more accurate mapping.

This analysis implies that chain back-folding (over length scales  $> D$ ) is costly, as demonstrated in a recent experiment on DNA.<sup>62</sup> The entropic penalty for back-folding is similar to what we would expect from a polymer ring. Accordingly, it supports the blob picture in which a linear chain under cylindrical confinement can be viewed as a linear string of blobs.<sup>1,6</sup> This picture also applies to each subchain of a ring. Linear ordering of these blobs is a natural consequence of a high free-energy penalty for back-folding. It also has physical consequences on chain miscibility or the way two confined chains interact, as detailed below.

**2.3.3 Flory approach to the extended de Gennes regime**—It proves useful to extend the Flory approach to the case where Kuhn segments are *asymmetrical* or self-avoidance is weak. A salient feature of such a chain under cylindrical confinement is the emergence of the extended de Gennes regime,<sup>15–17</sup> as briefly discussed in subsect. 2.2.2. In this subsection, we present a Flory approach to this case.

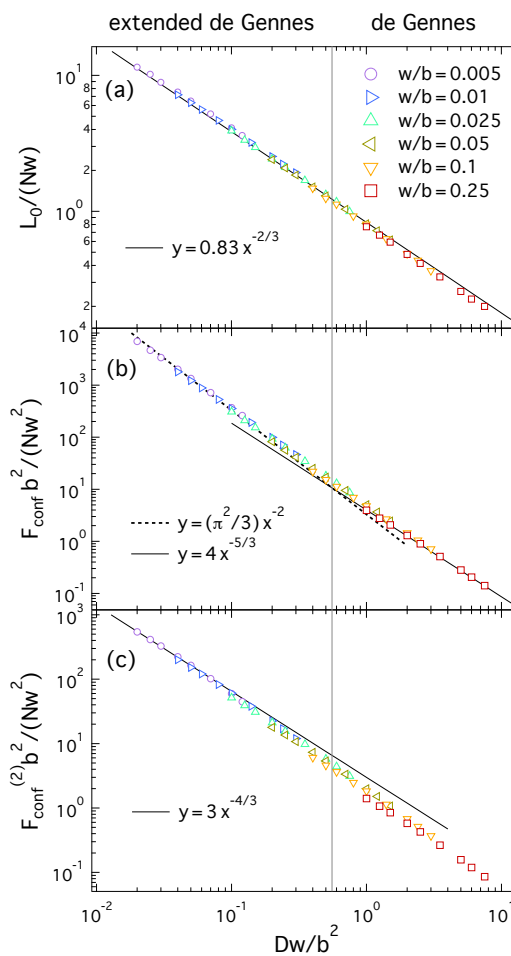


**Fig. 5** Simulation results for a freely-jointed chain of  $10^4$  rods, i.e.,  $N = 10^4$ , confined inside a narrow pore with a square cross-section [adapted from Ref.<sup>16</sup> Copyright (2014) American Chemical Society]. (a), (b), & (c) show the normalized extension, (b) normalized confinement free energy, and (c) the difference in confinement free energy between a real chain and an ideal chain, as a function of normalized pore width. Here the free energy is given in units of  $k_B T$ . The crossover between the extended and classic de Gennes regimes occurs at  $D_d = 0.56b^2/w$ , marked by the vertical straight line.

Let  $w$  be the thickness and  $b$  the Kuhn length. (For a spherical monomer,  $w = b = a$ .) Then  $p = b/w$  is the aspect ratio of Kuhn segments and  $v \approx b^2 w$  is the excluded volume parameter.<sup>2,63</sup> For a semiflexible chain of persistence length  $\ell_p$ ,  $b = 2\ell_p$  is the effective Kuhn length.<sup>3</sup> If  $L_{\text{total}}$  is the total contour length of the chain, the chain can be considered as being made of  $N = L_{\text{total}}/b$  rods of length  $b$  and thickness  $w$  each.

The Flory free energy of an unconfined chain reads

$$\frac{\mathcal{F}_{\text{Flory}}}{k_B T} \approx \frac{R^2}{N b^2} + v \frac{N^2}{R^3}. \quad (23)$$

Recall that  $\xi_T$  is the length of a thermal blob within which self-avoidance is irrelevant and  $g_T$  is the corresponding  $N$  value:  $\xi_T = b\sqrt{g_T}$ . If we use this in the second term of  $\mathcal{F}$  in Eq. 23 and set it to unity, we arrive at

$$\xi_T \approx p^2 w = \frac{b^2}{w}, \quad (24)$$

which is consistent with the known result.<sup>1,2</sup>

A related point is that the interaction energy (the second term in Eq. 23) evaluated at  $R_0 = \sqrt{N}b$  is proportional to the interaction parameter  $z$  in Eq. 2:  $z \propto \mathcal{F}_{\text{int}}(R_0)/k_B T \approx v N^2/R_0^3 = \sqrt{N}v/b^3$  ( $= \sqrt{N}v/a^3$  for spherical monomers). Setting  $z$  to unity (with  $N = g_T$ ) amounts to setting  $\mathcal{F}_{\text{int}}(R_0) = k_B T$ . Our analysis above is equivalent to the one carried out to obtain  $\xi_T$  below Eq. 2.

Now imagine squeezing the chain in a cylindrical pore of diameter  $D$ . As long as  $D \gg \xi_T$ , the general picture presented in subsec. 2.2.1 or 2.3.1 remains applicable. For instance, the confined chain is a linear array of blobs of size  $D$  each and  $\mathcal{F}_{\text{cyl}}$  in Eq. 17 remains valid – the only difference between the athermal and weak-self-avoidance cases is through  $g$ : in the latter case  $g \approx (D/b)^{5/3} (b^3/v)^{1/3} \approx (D/b)^{5/3} (b/w)^{1/3}$ , as can be readily obtained from Eq. 3. As a result,  $L_0 \approx (N/g)D \approx Nb(D/b)^{-2/3} (w/b)^{1/3}$  and  $k_{\text{chain}}/k_B T \approx N^{-1} b^{-2} (D/b)^{-1/3} (b/w)^{1/3}$ .<sup>13,15–17</sup>

If  $D$  is smaller than  $\xi_T$ , within a length scale  $D$ , the effect of self-avoidance is not significant. If we still insist on picturing the chain as a succession of possibly-overlapping spherical blobs of size  $D$  each, a few adjacent blobs can penetrate each other with no appreciable energy cost, as illustrated by the overlapping red dashed circles in Fig. 4(b). As a result, the chain becomes linearly arranged beyond  $\xi_{\parallel}$  beyond which self-avoidance becomes appreciable. Let  $N_{\parallel}$  be the corresponding number of Kuhn segments. Obviously, one can set  $\xi_{\parallel} \approx \sqrt{N_{\parallel}}b$ , since a chain with  $N < N_{\parallel}$  behaves as an ideal chain confined in the pore, i.e., the longitudinal size  $\langle X \rangle \approx \sqrt{N}b$  for  $N < N_{\parallel}$ .

Similar to the one used for  $\xi_T$ , one can set up an entropy-energy balance relation using Eq. 23 with  $R^3$  (in bulk) replaced

by  $D^2 R$  (in a pore):

$$v \frac{N_{\parallel}^2}{D^2 \xi_{\parallel}} \approx b^2 w \frac{(\xi_{\parallel}/b)^4}{D^2 \xi_{\parallel}} \approx 1. \quad (25)$$

This leads to

$$\xi_{\parallel} \approx \left( \frac{D^2}{bw} \right)^{1/3} b. \quad (26)$$

It is straightforward to see that  $\xi_T > \xi_{\parallel} > D$ . The first inequality is a natural consequence of confinement. First recall that both are defined as length scales beyond which self-avoidance becomes significant; if  $\xi_T$  is defined for an unconfined chain,  $\xi_{\parallel}$  is for a cylindrically-confined chain. This inequality means that self-avoidance becomes relevant at shorter (longitudinal) length scales for smaller  $D$ . On the other hand, the second inequality is consistent with the notion of anisometric or elongated blobs<sup>55</sup> (see also Refs.<sup>13,15,16</sup>).

Beyond  $\xi_{\parallel}$ , self-avoidance tends to stretch out the chain along the pore. The equilibrium (longitudinal) size of the chain is then given by

$$\begin{aligned} L_0 &\approx \xi_{\parallel} \times \frac{N}{N_{\parallel}} \approx Nb \left( \frac{v}{D^2 b} \right)^{1/3} \\ &\approx ND^{-2/3} b^{4/3} w^{1/3}. \end{aligned} \quad (27)$$

Except for a numerical prefactor, this is identical to  $L_0$  for the case  $D > \xi_T$ .

The boundary between the classic de Gennes and the extended de Gennes regimes can be obtained by setting  $\xi_{\parallel} = D$  (see Ref.<sup>55</sup>)

$$D \approx 0.56 \frac{b^2}{w}, \quad (28)$$

where the numerical prefactor was employed from Ref.<sup>16</sup> In a  $D$ - $w$  plane, this relation separates between the two regimes, as shown in Fig. 4(d). This relation has been confirmed in a recent numerical study,<sup>16</sup> as summarized in Fig. 5 (see below for details).

To proceed further, let us calculate the free energy of chain confinement  $\mathcal{F}_{\text{conf}}$ . To this end, we adopt two different pictures. First, we consider the chain as a linear array of many subsystems of size  $\xi_{\parallel}$  each and treat each subsystem as ideal. We then find  $\mathcal{F}_{\text{conf}}/\text{blob} \sim N_{\parallel} (b/D)^2$  (ideal inside  $\xi_{\parallel}$ ). The total free energy is then obtained as

$$\frac{\mathcal{F}_{\text{conf}}^{(1)}}{k_B T} \approx N_{\parallel} \left( \frac{b}{D} \right)^2 \times \left( \frac{N}{N_{\parallel}} \right) \approx N \left( \frac{b}{D} \right)^2. \quad (29)$$

This is the same as that of an ideal chain; chain elongation beyond  $\xi_{\parallel}$  will not change the scaling behavior of  $\mathcal{F}_{\text{conf}}$ . This is consistent with the earlier picture in subsubsec. 2.2.2 that the weak self-avoiding walker experiences a free energy cost of

$k_B T$  each time it travels a distance  $D$  (in the transverse direction).

In the second picture, we use Flory theory to calculate  $\mathcal{F}_{\text{conf}}$ . The self-avoidance contribution (thus  $\mathcal{F}_{\text{conf}}$ ) scales as

$$\frac{\mathcal{F}_{\text{conf}}^{(2)}}{k_B T} \approx \nu \frac{N^2}{D^2 L_0} \approx \frac{N b^{2/3} w^{2/3}}{D^{4/3}} \approx \frac{N}{N_{||}}. \quad (30)$$

The last relation tells us that the Flory approach is equivalent to assigning  $k_B T$  to each elongated blob of longitudinal size  $\xi_{||}$ .

Recently, a Flory free energy for the cylindrically-confined case has been constructed and tested numerically,<sup>16</sup> which is in our notation given by

$$\frac{\mathcal{F}_{\text{extended}}(X)}{k_B T} \approx \frac{N b^2}{D^2} + \frac{X^2}{N b^2} + \nu \frac{N^2}{D^2 X}. \quad (31)$$

The first term describes the free energy cost for squeezing a spherical thermal blob into a narrow cylinder. The second and third terms are analogous to the two terms in Eq. 23: if the second term represents a free energy cost for stretching the chain in the longitudinal direction, the third term describes excluded-volume interactions.

Minimization of this free energy leads to the expected  $L_0$ . But the confinement free energy,  $\mathcal{F}_{\text{conf}} = \mathcal{F}_{\text{extended}}(L_0)$ , is given by

$$\frac{\mathcal{F}_{\text{conf}}}{k_B T} \approx \frac{N b^2}{D^2} + \frac{N b^{2/3} w^{2/3}}{D^{4/3}}. \quad (32)$$

Note that this is a linear combination of the two free energy expressions in Eqs. 29 and 30. While it can be considered as a more complete form of confinement free energy for the extended de Gennes regime, in the limit  $\xi_T \approx b^2/w \gg D$ , this free energy is dominated by the first term.<sup>16</sup> For this, refer to Fig. 5 reproduced from Ref.,<sup>16</sup> which displays the simulated confinement-free energy against  $D$ . While the sum of  $\mathcal{F}^{(1)}$  and  $\mathcal{F}^{(2)}$  are shown in (b), the latter is displayed in (c). Clearly  $\mathcal{F}^{(1)}$  is an order of magnitude larger than  $\mathcal{F}^{(2)}$ .

In summary, the confinement free energy of a self-avoiding chain shows two scaling regimes:

$$\frac{\mathcal{F}_{\text{conf}}}{k_B T} \approx \begin{cases} N \left(\frac{b}{D}\right)^{5/3} \left(\frac{w}{b}\right)^{1/3} & \text{for } \xi_T < D < R_F \\ N \left(\frac{b}{D}\right)^2 & \text{for } D < \xi_T < R_F \end{cases}. \quad (33)$$

The confinement free energy for the extended de Gennes regime (the second line in Eq. 33) is approximately correct.

### 3 Confinement and molecular crowding

Large particles in a solution of small ones can attract each other, even if by themselves they would repel. The surrounding small particles induce entropic (depletion) forces between the large ones. The entropic origin of these forces can readily

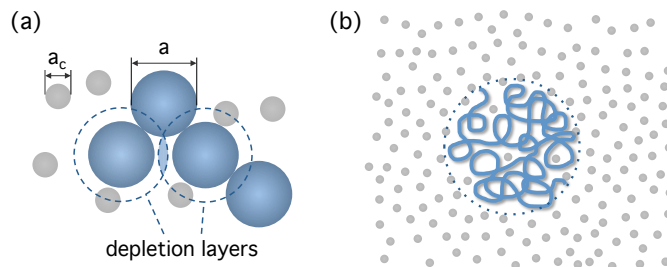


**Fig. 6** Depletion forces induced by crowding particles (in grey). (a) Each monomer (in dark blue) is surrounded with a depletion layer (dashed circles), in which the crowdors are excluded. Overlapping of depletion layers (shaded region) creates an extra space for crowdors. This induces entropic (depletion) forces between two monomers (or two large particles). (b) At a sufficiently large  $\phi_c$ , a chain molecule can be entropically phase-separated into a condensed state. Across the phase boundary (dotted line), crowdors are in chemical and mechanical equilibrium. As a result,  $\phi_c^{\text{out}} > \phi_c^{\text{in}}$ , where ‘in’ and ‘out’ refer to the inside and outside of the boundary.

be understood in terms of overlapping of ‘depletion layers,’ as illustrated for monomers in Fig. 6(a). A large particle is surrounded by a depletion layer inside which the center of small ones are excluded. As described in Fig. 6(a), association of two such particles leads to (partial) overlapping of their depletion layer, thus increasing the translational entropy of small ones.

A chain molecule can thus be compacted in a crowded medium, since its monomers will experience depletion forces, which compete with their excluded-volume interaction. Beyond a certain volume fraction of crowdors, the depletion force becomes dominant and collapses the chain, as illustrated in Fig. 6(b).<sup>27,64–75</sup> (See Refs.<sup>76–78</sup> for depletion forces in more general contexts). This phenomenon is somewhat analogous to chain collapse in a poor solvent<sup>52,79</sup> and is relevant to chromosome organization in cells, especially in bacterial cells. The bacterial chromosome is macroscopically long (about 2 mm for *E. coli*) along its backbone but is confined to an intracellular space of micron size, known as the nucleoid.<sup>27,66</sup> While the complete picture of chromosome compaction is still elusive, recent single-chromosome experiments suggest that depletion forces alone can condense the *E. coli* chromosomes to its *in vivo* size.<sup>14</sup> Indeed, cells are crowded with biomolecules such as proteins and RNA.<sup>27,66,80–84</sup> For instance, a typical *E. coli* cell contains  $\sim 10^6$  cytoplasmic proteins, occupying a large (about 20%) fraction of the cell volume.<sup>66,81,83</sup>

Molecular crowding is relevant in a variety of contexts. For instance, it influences molecular diffusion, biochemical equilibria, bimolecular aggregation, translation, and cell growth.<sup>81,82,85,86</sup> In particular, this effect enhances DNA looping and thus plays a favorable role in organizing chromosomes

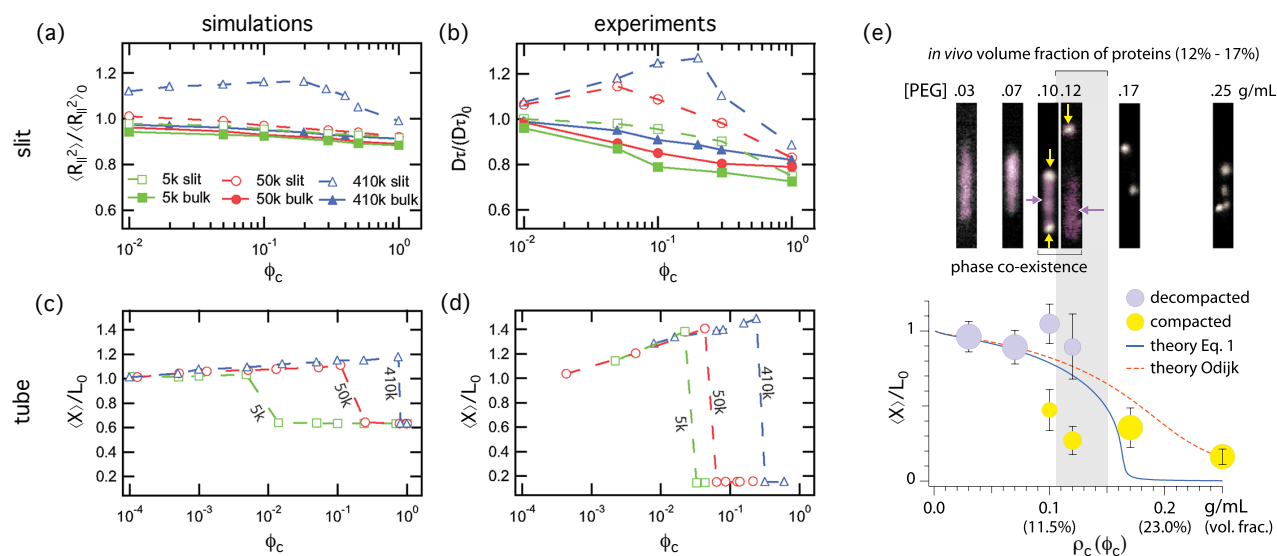


**Fig. 7** Results from Refs.<sup>14,72</sup> show how molecular crowding can condense chain molecules in a slit (a)(b) and a tube (c)(d)(e):  $\lambda$ -DNA in (a)-(c), T4-DNA in (d), and *E. coli* chromosomes in (e). In (a)-(d), the crowder used was dextran with variable molecular weights of 5, 50, and 410 kg/mol corresponding to the radius of gyration ( $R_g$ ) of 2.6, 6.9, and 17.1 nm, respectively. In (e), polyethylene glycol (PEG 2000) was used as crowding agents. The graph in (a) shows the mean squared radius of gyration from Brownian dynamic simulations ( $R_{\parallel}$  was the component of  $R_g$  in the direction parallel with the slit) and the graph in (b) displays the effective mean squared coil size for  $\lambda$ -DNA in bulk and slit channels of height 250nm from experimental measurements; here  $D$  is the diffusion constant of DNA, not to be confused with diameter,  $\tau$  is the rotational relaxation time, and the subscript refers to the case without crowders. Fig. (c) displays simulations of  $\lambda$ -DNA extension in tube (width 250 nm) and Fig. (d) represents experimental measurements of T4-DNA extension (tube width 300 nm)<sup>73</sup>. The graph in (e) shows the measured normalized extension of *E. coli* chromosomes in a pore with a cross-sectional area  $1.5 \mu\text{m} \times 1.7 \mu\text{m}$ ; the upper panel indicates a phase-coexistence at the volume fraction of crowders comparable to that of the cytoplasmic counterpart. In all these,  $\langle \dots \rangle$  represents an ensemble average quantity. [(a)-(d) adapted with permission from Ref.<sup>72</sup> Copyright (2011) American Chemical Society; (e) adapted from Ref.<sup>14</sup>]

in both eukaryotic and prokaryotic cells.<sup>85</sup> A seemingly adverse effect of molecular crowding is to limit translation and cell growth by hindering the diffusion of tRNA complexes.<sup>86</sup>

Nevertheless, in this section, we mainly focus on clarifying the role of molecular crowding in condensing chain molecules in a confined space. This effort will be beneficial for understanding the large-scale organization of bacterial chromosomes. More general discussions on crowding can be found elsewhere.<sup>65,78,79</sup> Furthermore, we do not attempt to resolve any discrepancy between competing views of chain compaction (e.g., continuous vs. abrupt). Indeed, the nature of chain compaction depends on various parameters including ion valence and chain stiffness. An abrupt transition of DNA was seen in a crowded medium containing negatively-charged proteins<sup>74</sup> as well as in polyethylene glycol (PEG) solution<sup>75</sup> (both in an unconfined space.) A more recent study, however, indicates a continuous DNA compaction by dextran (polymeric crowder) in an unconfined space or in a slit-like space but an abrupt transition in a tube-like space<sup>72,73</sup>; an abrupt transition was observed with *E. coli* chromosomes trapped in narrow pores.<sup>14</sup>

Fig. 7 summarizes recent results from Refs.<sup>14,72,73</sup> for chain compaction by molecular crowding in a confined space (slit- or tube-like). Fig. 7(a)-(d) describes the condensation of  $\lambda$ -DNA (48.5 kbp) by dextran \*\* in a slit-like (upper) or tube-like (lower) geometry; if the slit height is 250 nm, the tube width is 300 nm. (For other details, refer to the original papers.<sup>14,72,73</sup>) Also what is shown in (b) is the effective mean squared coil size, where  $D$  is the diffusion constant of DNA, not to be confused with diameter,  $\tau$  is the rotational relaxation time, and the subscript refers to the case without crowders. Fig. 7(e) represents *E. coli*-chromosome compaction in a cylindrical channel.

In all cases, the chain molecules undergo a coil-to-collapse transition as the volume fraction of crowders  $\phi_c$  increases. DNA compaction in a slit-like space is continuous as in bulk (bulk data represented by filled triangles in (a)(b)), but it is abrupt in a tube-like space. Intriguingly, the dependence of chain sizes on  $\phi_c$  is non-monotonic for some curves in (a) and (b), and for all curves in (c) and (d). The initial elongation of DNA molecules can be understood in terms of the following physical picture: DNA segments are depleted in a (depletion) layer of some thickness on the order of  $\ell_p$  from the confining wall,<sup>72,73</sup> where  $\ell_p \approx 500 \text{ \AA}$  is the persistence length of DNA. This allows for an easy access of crowders in this depletion layer, effectively increasing the degree of confinement – more so for a larger  $\ell_p$ .

Indeed, this non-monotonic behaviour was considered to be implicated in the abrupt transition seen in (c) (simulations) and (d) (experiments). Under cylindrical confinement, the effect

of crowders is anisotropic: it initially compresses the DNA molecules radially but eventually acts to collapse them in the longitudinal direction. This explains why the compaction transition of DNA molecules is more cooperative and abrupt in tube-like confinement.<sup>72,73</sup>

Similarly, the compaction of *E. coli* chromosomes in a tube-like space appears to be abrupt, as it suggests coexistence of compacted and extended phases (see Fig. 7(e)). However, this does not appear to be correlated with chain-segment depletion from the wall seen in (a)-(d), since the chain length shrinks monotonically, as the volume fraction of crowders increases. Along this line, it is worth noting that the “effective” Kuhn segments of chromosomes are not as anisotropic as those of DNA. As detailed later (as also illustrated in Fig. 1(b)), the bacterial chromosome is organized by various proteins into topologically-independent domains or structural units,<sup>26–28</sup> which can be approximated as effective monomers.<sup>14,21,22</sup> It can behave differently from what we would naively expect from the physical picture of DNA molecules. This may be responsible for the difference between the DNA and chromosome experiments in Fig. 7. Also the chromosome is structurally (more) heterogeneous along its backbone (than DNA). This is also expected to be implicated in the observed phase coexistence in Fig. 7(e).

Also superimposed are theoretical results based on polymer-chromosome models: if the blue curve corresponds to a bead-spring model, the red dashed line represents a cross-linked polymer (see Ref.<sup>14</sup> and references therein). While both curves indicate a continuous transition, the blue curve compares more favorably with the experimental data. Furthermore, recent numerical and theoretical studies suggest that flexible-chain compaction is continuous in a cylindrical space<sup>35</sup> as well as in an unconfined space.<sup>87</sup>

There is now a considerable appreciation for crowding effects in organizing chain molecules, especially in a confined space. What remains to be further clarified is the nature of chromosome compaction. For a more complete understanding, it will be useful to examine how the compaction is influenced by chain stiffness and heterogeneity as well as by the size and poly-dispersity of crowders. Indeed, the cytoplasmic space presents a poly-disperse space, containing a mixture of various types of crowders.<sup>81,83</sup> Finally, crowders can also induce depletion forces between monomers and the confining cylindrical wall, possibly leading to chain adsorption onto the wall. It will be useful to discuss the effect of crowder's poly-dispersity as well as the interplay between chain adsorption and compaction: the emerging physics and biological implications (see Ref.<sup>35</sup> for recent efforts along these lines).

\*\* Dextran is a neutral branched polymer formed by glucose monomers. The size of dextran molecules used in Ref.<sup>73</sup> is in the range 2.6–17 nm.

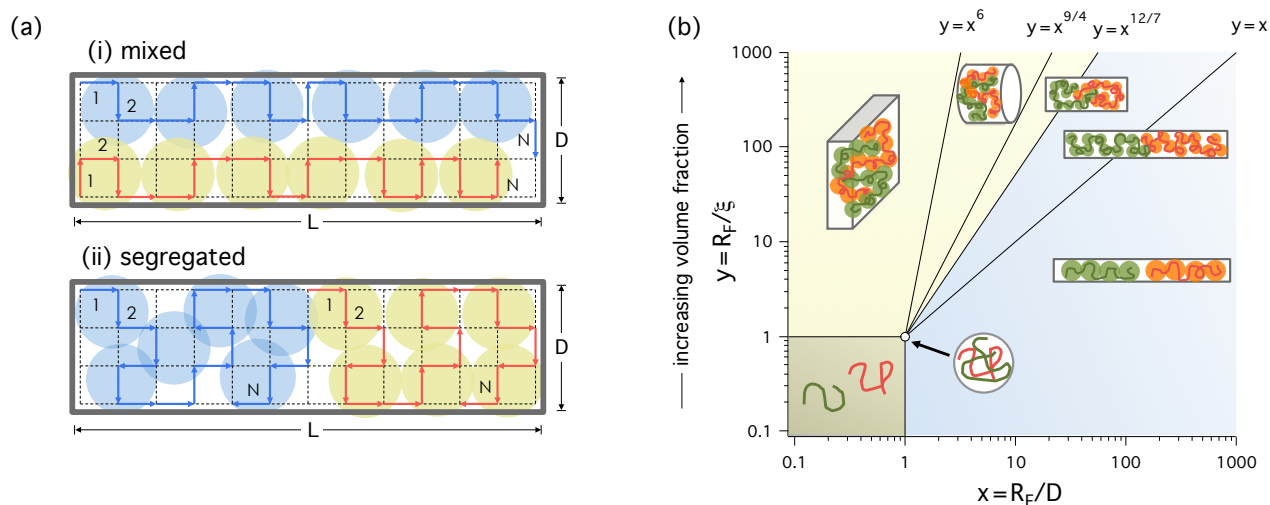


**Fig. 8** (a) Blob picture of two hypothetical self-avoiding chains, each having taken  $N$  steps on a lattice in a confined space: (a) mixed and (b) segregated. For simplicity, assume that  $L = L_0$  in the mixed case in (i), where  $L$  is the length of the confined space and  $L_0$  is the equilibrium chain length. The confined chain in (i) is a linear array of blobs, described by filled circles. The degree of linear ordering is diminished in (ii). It can be shown that entropy favors the segregated case in (ii). To see this, consider an imaginary chain formed by blobs, i.e., a string of blobs in (a). The conformational entropy of this blob-chain is minimal in (i) but is more appreciable in (ii). Note that the conformation shown in (ii) is one of several realizations; for instance, the two blob-chains on the left and right are different. As  $L$  decreases, however, the difference in blob-chain entropy between (i) and (ii) becomes less significant. As a result, they mix better. In principle, this line of reasoning leads to a diagram shown in (b),<sup>19</sup> which is based on the diagram for a similar problem: polymers trapped in pores in chemical equilibrium with those in a reservoir.<sup>7,8</sup> [The illustration in (b) is adapted by permission from Macmillan Publishers Ltd: Nat. Rev. Microbiol.,<sup>19</sup> copyright (2010).]

#### 4 Two-chain case

Much attention has also been placed on chain segregation or mixing in a confined space (e.g., slit-like, cylindrical, and spherical).<sup>7,8,19,21,22,44,88–90</sup> Cylindrical (anisotropic) confinement is of particular interest; it is not only a classic problem in polymer physics pioneered by de Gennes and his collaborators<sup>7,8</sup> but a problem of renewed interest because of its relevance to chromosome segregation in elongated bacterial cells.<sup>19,21,22,44</sup> Indeed, closed cylindrical confinement with a varying aspect ratio includes spherical confinement as a special case.

In this section, we discuss some of recent progress with (two) interacting chains in a confined space. Our consideration in this section is, however, limited to the case of strong-self-avoidance (see Ref.<sup>91</sup> for stiff-chain segregation). Chain segregation in an open cylindrical space is obvious to understand, as discussed above (recall  $\mathcal{F}_{\text{mix}} = 2^{1/2\nu} \mathcal{F}_{\text{seg}} > \mathcal{F}_{\text{seg}}$  in Eq. 10). In contrast, chains tend to mix under spherical confinement, as long as they are in equilibrium and are not kinetically trapped in a local free-energy minimum.

Closed cylindrical confinement combines both cases (open cylinder and sphere) and thus offers a richer set of segregation behavior. As an instructive model, consider the hypothetical polymer system shown in Fig. 8(a): two self-avoiding chains

on a lattice in a confined space. If the chains in the upper panel (i) are mixed, they are segregated in the lower panel (ii). For simplicity, assume that the cylinder length  $L = L_0 = \langle X \rangle$  in the mixed case in (i). As shown in the figure, the chains in (ii) are more randomly organized. It can be shown that entropy favors the segregated case in (ii). To see this in a more transparent way, consider an imaginary chain formed by blobs, i.e., a string of blobs. The conformational entropy of this “blob-chain” is minimal in (i) but is larger in (ii). The conformation shown in (ii) is one of several realizations; indeed, the two blob-chains on the left and right are different. This explains segregation is entropically favored, under the right conditions.

As  $L$  decreases, however, the difference in blob-chain entropy between (i) and (ii) in Fig. 8(a) becomes less significant. As a result, they will mix better, as  $L \rightarrow D$ . In principle, this line of reasoning leads to a diagram in which the degree of chain overlapping is depicted, as shown in Fig. 8(b),<sup>19</sup> which is based on an earlier study of a similar problem: polymers trapped in pores in chemical equilibrium with those in a reservoir.<sup>7,8</sup> (See the Supplementary Information of Ref.<sup>19</sup> for the details.) In this diagram, the boundary between different regimes is represented by a simple scaling relation between  $x = R_F/D$  and  $y = R_F/\xi$ , where  $R_F$  is the Flory radius (e.g., Eq. 3) and  $\xi$  is the blob size (Eq. 11). Since the scaling picture leading to chain segregability is discussed in detail else-

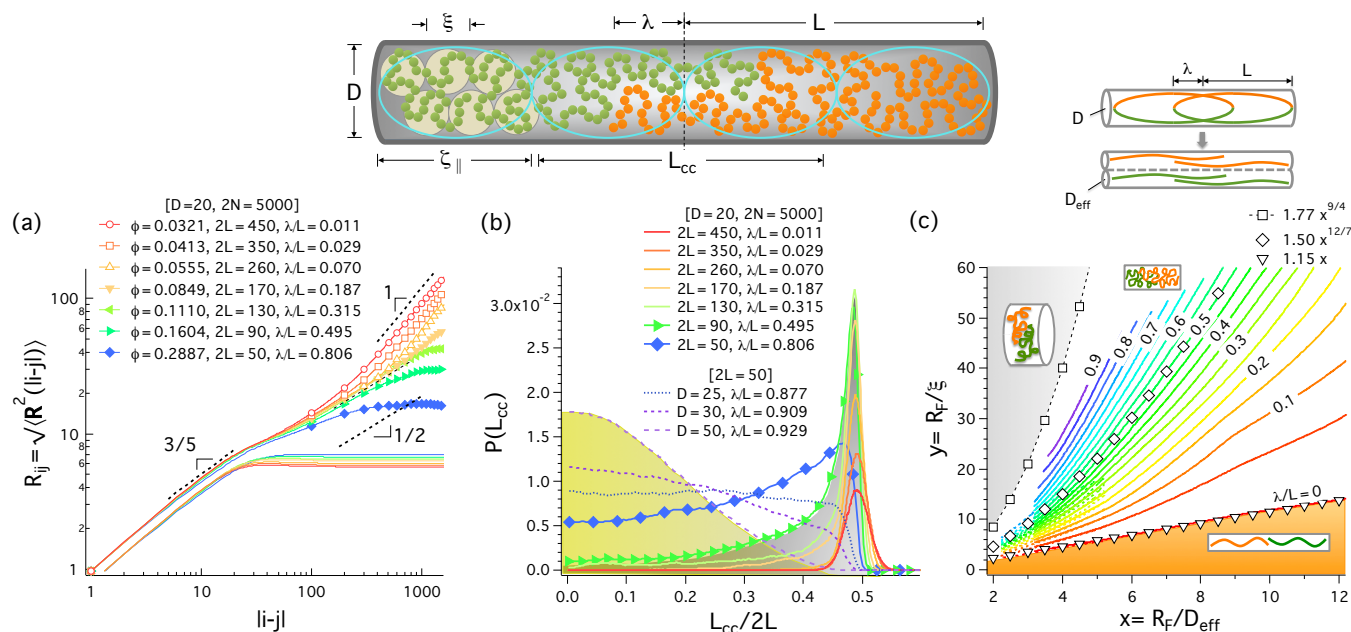


**Fig. 9** (a) Internal distance of a confined chain  $R_{ij} = \sqrt{\langle \mathbf{R}^2(|i-j|) \rangle}$  (solid lines with symbols) and its relationship with  $\lambda/L$ , the fractional overlap distance between two chains (specified in the legend) for  $D = 20a$  [adapted with permission from Ref.<sup>22</sup> Copyright (2012) American Chemical Society]. Here  $D$  is defined as the inner cylinder diameter and  $L$  is the cylinder length per chain. The color scheme is the same for all these graphs in (a)(b)(c). (a) The dashed lines, with the slopes  $3/5$ ,  $1/2$ , and  $1$ , depict the self-avoiding walk (SAW) within  $\xi$ , random walk (RW) at intermediate lengths, and linear regimes, respectively. If the confined chain is weakly compressed longitudinally, it is linearly ordered beyond the blob size  $\xi \approx D$ , as in an open cylinder, and the RW regime is missing. For moderate compression, blobs are randomly packed within some length scale  $\zeta_{||}$ ; linear ordering emerges beyond this. For strong compression, the linear regime disappears (i.e.,  $\zeta_{||} \approx L$ ). For the entire range shown, the RW regime is not clearly seen in the transverse component  $R_{ij}^{\perp} = \sqrt{\langle \mathbf{R}_{\perp}^2(|i-j|) \rangle}$  (the bottom lines without symbols). In all cases that display the linear regime in (solid lines unfilled symbols), the chains are (almost) completely segregated. Even when linear ordering is completely lost, they segregate up to 70-80%, more so in a more asymmetrical space. Under anisotropic confinement, chain segregation in the RW regime is sensitive to the aspect ratio  $r = D/L$ . (b) For the well-segregated cases (solid lines without symbols), the probability distribution of the center-to-center distance between the two chains  $P(L_{cc})$  has a narrow peak at  $L_{cc}/2L \approx 0.5$ . On the other hand,  $P(L_{cc})$  for the much mixed cases (lines with filled diamonds) is broader. In the most miscible case  $D/2L = 1$  (the dashed line in purple),  $P(L_{cc})$  is a Gaussian distribution centered at  $L_{cc} = 0$ . (c) In the diagram,  $D_{eff} = D$  for linear chains (solid lines), while for ring polymers,  $D_{eff} = D/\sqrt{2}$  (dashed lines).<sup>21</sup> The dotted line with open squares describes the symmetrical case of  $D/2L = 1$  for which  $y = 1.40 \times x^{9/4}$ . Beyond this, the confined space resembles a closed “slit.” Also included is the boundary curve  $y = 1.50 \times x^{12/7}$  between the segregated and mixed regimes<sup>7,8,19</sup> (see open “diamonds”), on which  $\lambda/L = 0.5$ . Finally,  $\lambda/L = 0$  line is best fit by  $y = 1.15 \times x$  (open inverted triangles).

where,<sup>7,8,19</sup> we do not repeat it here. Instead, we will include below the numerical support for the diagram (see Fig. 9(c)).

Furthermore, an earlier study shows how intra-chain and inter-chain ordering are interrelated.<sup>21</sup> Chains remain segregated effectively if linearly-ordered, as illustrated in Fig. 8(a)(b). They can resist mixing even outside the linear regime. This deviates somewhat from an earlier scaling prediction that segregation requires linear ordering<sup>7,8</sup> but is consistent with what was observed in a polymer melt.<sup>88</sup>

As a confined chain is compressed longitudinally, the blobs break into smaller ones and the degree of linear ordering decreases. Intrachain ordering can be quantified in terms of the internal distance between two monomers at  $i$  and  $j$ , given by

$$R_{ij} = \sqrt{\langle \mathbf{R}^2(|i-j|) \rangle}, \quad (34)$$

as introduced in subsec. 2.2. Related quantities are the internal distances measured in the longitudinal and transverse direction, respectively,

$$R_{ij}^{\parallel} = \sqrt{\mathbf{R}_{\parallel}^2(|i-j|)} \quad \text{and} \quad R_{ij}^{\perp} = \sqrt{\mathbf{R}_{\perp}^2(|i-j|)}. \quad (35)$$

Fig. 9(a) shows  $R_{ij}^{\parallel}$  (curves with symbols) and  $R_{ij}^{\perp}$  (curves without symbols).<sup>22</sup> It should be noted that the color scheme for  $R_{ij}^{\perp}$  curves is in error in the original work<sup>22</sup>; it should be reversed as in Fig. 9(a) in this work. Also in Fig. 9,  $D$  is defined somewhat differently from the one in Fig. 2(a). In Fig. 9, it is the inner diameter of the cylinder as shown in the illustration on the top. We have checked that the miscibility in Fig. 9(c), for instance, is largely insensitive to the way  $D$  is defined.

A few distinct regimes are marked in Fig. 9(a) (see the dashed lines with slopes in a log-log plot): self-avoiding (within  $\xi$ ), random-walk (at intermediate length scales), and linear regimes (outside the random-walk regime). Note that not all these regimes are always realized. Also  $L$  here is the length of the cylinder per chain. For large  $L$ , the chain is linearly organized beyond  $\xi \approx D$ , as in an open cylinder. As  $L$  decreases, a new regime between the self-avoiding and linearly-organized regimes emerges. In the log-log plot, this regime is described by a linear line with a slope 1/2. A natural consequence of chain compression is the emergence of a new length scale denoted as  $\zeta_{\parallel}$ . This is a length scale within which the confined chain ( $L < L_0$ ) is a random packing of compression blobs of size  $\xi$  each ( $\xi < D$ ). Beyond  $\zeta_{\parallel}$ , the chain is linearly organized, as long as  $\zeta_{\parallel} < L$  (see Fig. 9(a)). As  $L$  decreases,  $\zeta_{\parallel} \rightarrow L$ . In this case, linear ordering is completely lost as in a spherically-confined case.

The results in Fig. 9(b)(c) relate intrachain ordering to the degree of chain overlapping or penetration, which is measured by the probability distribution of the center-to-center distance between the two chains  $P(L_{cc})$  in Fig. 9(b) and the partial

overlap distance  $\lambda/L$  in Fig. 9(c); here  $\lambda$  is the overlap distance or penetration depth, not to be confused with the deflection length  $\lambda_{\text{def}}$  introduced in subsubsec. 2.2.2. In Fig. 9(c),  $R_F = \text{const.} \times 1.1N^{3/5}$ , where  $\text{const.} = 1$  or  $0.79$  for a linear or ring chain, and  $\xi = \phi^{-3/4} = [N/\pi(D/2)^2L]^{-3/4}$  (Eq. 11) with the prefactor set to unity was used.<sup>21</sup> (The prefactor  $0.79$  for  $R_F$  coincides with the ratio of the radii of gyration of the ring and linear chains.<sup>21</sup>) For linear chains,  $D_{\text{eff}} = D$  by convention. The color scheme used for various curves is the same for all the graphs in Fig. 9(a)(b)(c). When the chain is linearly organized in the sense that  $\zeta_{\parallel} < L$ , the two chains remain segregated. It is worth noting that for  $\lambda \approx 0.5$ ,  $P(L_{cc})$  has a peak around  $L_{cc} = L$  (see the green curve in (b)). While on average the chains penetrate each other halfway through, the most probable conformation represents segregation. In this case, linear ordering is completely lost as indicated in Fig. 9(a). But the chains still resist mixing (they are half-segregated). Only when the chains mix almost completely, the peak moves to  $L_{cc} \simeq 0$ . (The three dashed lines in (b) show how the chains mix as the aspect ratio  $2L/D$  tends to unity.)

Also shown in Fig. 9(c) is the boundary curve between the two neighbouring regimes. For instance, the dotted line with open squares describes the symmetrical case of  $2L/D = 1$  for which  $y = 1.40 \times x^{9/4}$ . Beyond this, the confined space resembles a closed ‘‘slit.’’ On the other hand, the boundary curve  $y = 1.50 \times x^{12/7}$  distinguishes between the segregated and mixed regimes<sup>7,8,19</sup> (see open ‘‘diamonds’’); on this boundary curve,  $\lambda/L = 0.5$ . Finally, the  $\lambda/L = 0$  line corresponds to  $y = 1.15 \times x$  (open inverted triangles). These boundary curves are consistent with and offer numerical support for those based on the scaling picture.<sup>7,8,19</sup>

Intriguingly, it was shown that a ring polymer behaves as a series connection of two sub-linear chains, each trapped in an imaginary narrower cylinder of diameter  $D_{\text{eff}} = D/\sqrt{2}$ , as illustrated in Fig 9(c).<sup>22</sup> In the figure, the dashed lines describe two ring polymers. The collapse between the linear and ring cases means that the effect of ring topology is correctly mimicked this way and that ring polymers segregate better than the corresponding linear chains. For practical purposes, one can use the same  $\xi$  value for the linear and ring cases, as done in Fig. 9. This is obvious for  $L_{\text{linear}} > L_{\text{ring}} \geq L$ , where  $L_{\text{linear}}$  or  $L_{\text{ring}}$  is the equilibrium chain size for the linear or ring case, respectively, introduced in subsec. 2.3.2. If so, the monomer volume fraction is the same in both cases; so is  $\xi$ . If  $L_{\text{linear}} > L \geq L_{\text{ring}}$ , however, the ring polymers can fall below the  $\lambda/L = 0$  boundary, even though the linear chains remain touched. The use of the same  $\xi$  can be justified if the linear chains remain segregated. Indeed, this is the case, since there is a good agreement between the solid (linear) and corresponding dashed (ring) lines even for  $\lambda/L \simeq 0$ . For the comparison purpose, one can use the same  $\xi$  for both cases.

This physical picture is consistent with the observation that

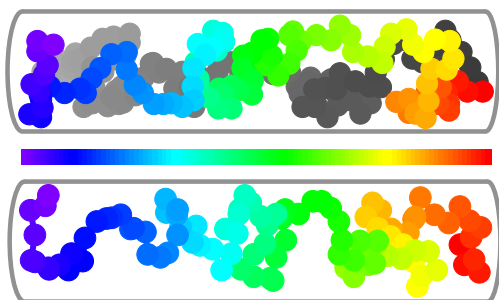


**Fig. 10** Linear ordering of a polymer ( $N = 200$ ) in a closed cylindrical space of length  $L = 28$  and diameter  $D = 4.8$  for  $N = 200$ , adapted from Ref.<sup>21</sup> by permission of the Royal Society of Chemistry. A typical chain conformation is shown. The beads are colored in the same sequence as in the color bar in the middle. For a ring polymer (the upper figure), only one subchain shows up in color. The lower panel displays a linear subchain (consisting of  $N/2$  monomers) trapped in a narrow cylinder with a rescaled diameter as  $D \rightarrow D/\sqrt{2}$ . The cylinder diameter was exaggerated so that it matches with that in the ring case. Because of the  $D$  rescaling, the chains in the two cases are similarly organized. The degree of linear ordering shown here is comparable to the following scaled-down case:  $N = 100$ ,  $D = 4.8$ , and  $L = 14$  (more suitable for the *E. coli* nucleoid (see Sec. 5)).

ring- or loop-like structures of individual chains induce a repulsion between them, similarly to what is seen in interphase chromosomes in a eukaryotic cell, forming discrete territories.<sup>41,89,90</sup>

Along this line, it is worth noting that overlapping two chains in a free or spherical space is not completely free but can be a few  $k_B T$ .<sup>41</sup> As the degree of topological complexity increases, the overlapping free energy will also increase and the chains segregate better.<sup>19,44</sup> In this regard, the results in Fig. 9 can be considered as a lower bound for the segregability of chains with nontrivial topology (e.g., chromosomes).

## 5 Polymer physics approach to bacterial chromosomes

The physical picture of linear ordering and chain segregation induced by cylindrical confinement has been used as a physical basis of chromosome organization and segregation in elongated bacteria.<sup>19,21,22,44</sup> Varying views have also emerged, in which (possible) limitations of polymer approaches are pointed out or the roles of chromosome-associated proteins are emphasized.<sup>92–95</sup> This is not surprising, considering the complexity of chromosomes in comparison with polymers. For the same reason, simplification is an inevitable step toward gaining quantitative insight. The degree of simplification should reflect the desired level of abstraction. Polymer

models have emerged as a minimalist but nontrivial physical model of chromosomes, since they still retain such essential features as chain connectivity and excluded volume interactions between chain segments (chain topology as well in some case)<sup>19,21,22,44</sup> (also see Refs.<sup>89,90</sup>). Importantly, a polymer model offers a conceptual framework for making quantitative sense of chromosome experiments (see Ref.<sup>14</sup> for a recent attempt).

Here, we briefly review some of the discussions along this line in the literature. However, we do not attempt to resolve any “essential” discrepancy between the varying views, e.g., active or protein-assisted vs. passive or entropically-driven segregation of chromosomes (see Refs.<sup>19,20,92,93</sup> and references therein for relevant discussions). However, we believe that some of them are only *deceptively* contradictory. Where applicable, we clarify the nature of discrepancies.

### 5.1 The bacterial chromosome and a polymer model

The bacterium *E. coli* has a circular chromosome, carrying about  $4.6 \times 10^6$  base pairs. It is about 1.6 mm along its contour and experiences about 1000-fold compaction inside the cell, occupying an intracellular space known as the nucleoid.<sup>27,96</sup> However, even with this spatial constraint, the bacterial DNA is highly active in gene expression, replication, and segregation.<sup>29,93,97</sup>

The bacterial chromosome is compacted in part by the negative supercoiling of DNA into many topologically-independent domains or structural units;<sup>26–28,98–100</sup> these domains and their boundaries are highly dynamic.<sup>28</sup> Beyond this generally accepted picture, their details vary from reference to reference. For instance, it was shown in Ref.<sup>28</sup> that each domain is about 10-kb (kilo-base-pair) long, implying that the chromosome contains about 400 structural units. In Ref.,<sup>101</sup> each structural unit was estimated to be  $70 \pm 20$  nm in diameter and 50 kb in length; the number of structural units falls around 100. More recent single-molecule experiments led to somewhat larger structural units ranging from 130 nm to 440 nm, together with the number of structural units in the range 15–65 per chromosome (63–284 per cell)<sup>14, ††</sup>

The organization of bacterial chromosomes<sup>102–105</sup> as well as the cell/nucleoid sizes depend on growth conditions and cell ages or vary from reference to reference.<sup>27,93,94,96,106</sup> The *E. coli* chromosome resembles a donut (or a branched donut<sup>105</sup>), under fast-growth rates, but it is asymmetrically organized, resembling a ‘sausage’ with a stretch connecting its ends, under slow-growth rates.<sup>102–104</sup> The donut-like chromosome bears a resemblance to the ring polymer in the upper panel of Fig. 10. Imagine shrinking the size of monomers shown in a varying

†† As noted below, an *E. coli* cell contains more than one chromosomes, depending on cell growth conditions.

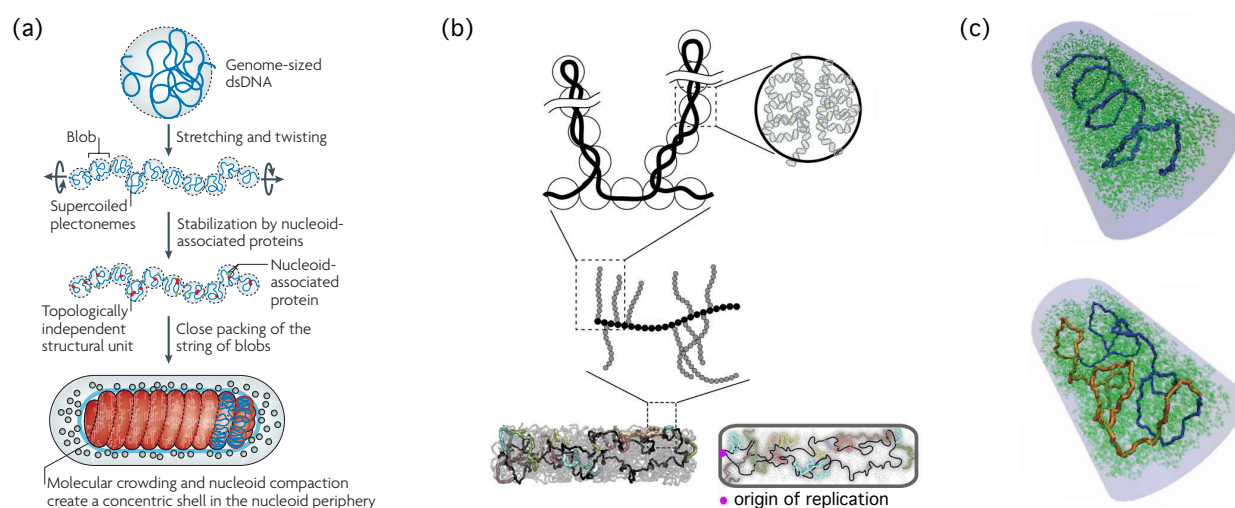


**Fig. 11** Organization of the bacterial chromosome into the nucleoid and coarse-grained polymer models of the chromosome: a simple polymer (a) and bottle brush-like fiber (b)(c), modified from Ref.<sup>19</sup> and Refs.,<sup>108,109</sup> respectively. (a) The linear or ring polymer model of the *E. coli* chromosome. Note that the mapping is not necessarily unique: the structural unit is interpreted as a blob in Ref.<sup>19</sup> but as a monomer in Refs.<sup>21,22</sup> Also the size and number of units vary appreciably from reference to reference (see the text for details); so do the size and number of monomers in the polymer model. (b) The bottle brush<sup>108</sup> that models the *Caulobacter* chromosome consists of a backbone chain and side loops (supercoiled plectonemes) emanating from the backbone; each plectoneme is formed by 35 monomers on average, with each monomer 13.7 nm in diameter and containing 434 bp of DNA. The resulting bottle brush consists of 9,274 monomeric units and is confined inside a cell-mimicking, cylindrical space (which is 450 nm in diameter and 2500 nm in length). (c) Organization of a bottle-brush polymer in a confined space. The backbone is helically organized for both linear (upper) and ring (lower) backbones. [(a) is adapted by permission from Macmillan Publishers Ltd: Nat. Rev. Microbiol.,<sup>19</sup> copyright (2010); (b) from Ref.<sup>108</sup> Reprinted with permission from AAAS. (c) Copyright (2012) by The American Physical Society.]

grey scale in the panel. The resulting asymmetrical ring is analogous to the sausage-like chromosome.

For new born-cells under slow-growth rates, containing single sausage-like chromosomes, the measured nucleoid dimensions range from  $1.64\mu\text{m} \times 0.48\mu\text{m}$ <sup>93</sup> to  $1.8\mu\text{m} \times 0.8\mu\text{m}$ .<sup>94</sup> These are somewhat different from the earlier measurement of  $1.39\mu\text{m} \times 0.24\mu\text{m}$ <sup>‡‡</sup>.<sup>27</sup> Fast-growing cells are somewhat larger and contain constantly-replicating chromosomes.<sup>105</sup>

In polymer chromosome models,<sup>19,21,22,44,92,94</sup> such molecular details as supercoiling and other activity of DNA-bound proteins are often coarse-grained into monomers. The local structure of a chromosome can be effectively influenced by these molecular details, but its global property is expected to be much less sensitive to the details. This is a distinguishing feature of chain molecules<sup>1,3</sup> and may justify the use of a coarse-grained chromosome model (e.g., a polymer model). Below we collect a few polymer models.

Perhaps, the simplest model amounts to coarse-graining the structural unit as a monomer. The structural units are topologically constrained and can be approximated as impenetrable spheres, as illustrated in Fig. 1(b), where the genomic length DNA is organized into a string of many structural units or monomers.<sup>21,22,30</sup> (More realistically, one can use a circular string of monomers. Also see Fig. 11(a) for an alternative view of the structural unit.<sup>19</sup>) In this case, the size and number of monomers will be set by the size and number of structural units, as discussed above. The bending stiffness of double stranded (ds) DNA is not a crucial parameter, since each structural unit contains many persistence lengths, each  $\ell_p$  about 150 bp long.<sup>107</sup> While the local stiffness of the DNA influences how it interacts with proteins, its effect will not persist much beyond  $\ell_p$ . The resulting polymer model, i.e., beads (structural units) on a string, with linear or ring topology, has been used in a number of recent studies.<sup>21,22,44</sup> It is unlikely that the extended de Gennes regime will be realized for this, considering the overall spherical shape of each monomeric unit.

An obvious variation of the simple bead-string model is to include explicitly cross-links between chain segments or non-trivial chain topology induced by supercoiling, as shown in Fig. 1 (lower panel) and Fig. 11(b)(c) (see below for more details). Indeed, the choice of a polymer chromosome model should depend on the nature of questions one wishes to address (e.g., “What is the role of cross-linking proteins in the large-scale organization of chromosomes?”).

## 5.2 Spatial organization of bacterial chromosomes vs. polymers

### 5.2.1 Single chromosomes—Fluorescence imaging techniques showed that a single chromosome before the onset of

‡‡ As pointed out in Ref.<sup>19</sup>, the nucleoid length  $1.39\mu\text{m}$  is somewhat smaller than the population average  $1.9\mu\text{m}$

DNA replication in a slowly growing *E. coli* cell is linearly organized along the long cell length<sup>110–113</sup> (with a stretch of segments connecting the two poles of the packed chromosome). On the other hand, linear ordering of a chain molecule in a cylindrical space is now obvious.<sup>19,21,22,44,114</sup> In an earlier study,<sup>21</sup> linear ordering was observed for a ring polymer, consisting of 200 monomers, trapped in a cylinder of diameter  $D = 4.8$  and length  $L = 28$  (in units of monomer size), as shown in Fig. 10; for these choices,  $L_0 \approx 41$ . As a result, the aspect ratio  $L/D$  is about two times as big as expected for the *E. coli* nucleoid. However, the degree of linear ordering in this case should be comparable to what we would expect from the following scaled-down case: a chain consisting of 100 monomers, trapped in a cylinder of diameter  $D = 4.8$  and length  $L = 14$ . Note that these choices fall in the acceptable parameter ranges for the *E. coli* chromosome, if viewed as beads (structural units) on a string. This analysis appears to be consistent with the observation of linearly ordered *E. coli* chromosomes.<sup>113</sup>

However, the onset of linear ordering will depend on several molecular details including cross-linking (see the relevant illustration in Fig. 1(a)) and tethering of the chromosome to the cell membrane.<sup>19,23</sup> As for a simple polymer inside a closed cylinder, it is set by the single-length scale  $\zeta_{||}$ , as shown in Fig. 9. In our polymer picture, cross-linking between proximate segments along the contour can be considered as shortening  $\zeta_{||}$ , diminishing the local positional fluctuation of monomers. As a result, monomers will be more precisely positioned. Indeed, a recent computational study shows that the introduction of cross-links at appropriate genomic positions in an otherwise simple polymer improves the precision with which loci are spatially distributed, similarly to what was observed with the *E. coli* nucleoid.<sup>23</sup>

Along the line of discussions above, it is worth repeating the intrachain organization analysis in Fig. 9(a) for a wider range of polymer-cylinder parameters. What is clear is that  $\zeta_{||}$  is smaller for smaller  $N$  (assuming  $L < L_0$ , where  $L_0$  is either  $L_{\text{linear}}$  or  $L_{\text{ring}}$ ). As a result, enhanced linear ordering by cross-linking is analogous to reducing  $N$  in a linear or ring polymer, in the sense that the onset of linear ordering starts at a shorter length scale; in this case,  $a$  may have to be increased, since each monomer now includes more molecular details (more DNA segments and associated proteins).

In a recent work,<sup>92</sup> a lengthwise (orderly) folding of adjacent DNA segments (clustering of proximate segments along the contour more closely) is attributed to the linear ordering of chromosomes and their segregation. (This is also reflected in the illustration in Fig. 11(a).) In light of our discussion on  $\zeta_{||}$  above, we believe that this picture does not necessarily contradict confinement-induced linear ordering. The lengthwise folding can be considered as shortening  $\zeta_{||}$ , which can also be achieved by reducing  $N$ .

**Table 1** Miscibility vs. the aspect ratio  $r = L/D$  for  $N = 100$  and  $D = 5$ . The data with  $r = 3$  represent the *E. coli* chromosome better than others. Confined chains segregate better with ring topology or for larger  $r$ .

chain topology	aspect ratio $r$	$x = R_F/D$	blob size $\xi$	$y = R_F/\xi$	degree of overlap $\lambda/L$
linear	6	4.40	4.97	5.32	complete segregation
	5		4.34	6.10	complete segregation
	4		3.67	7.21	5% overlap
	3		2.96	8.94	10% overlap
	2		2.18	12.1	25% overlap
ring	6	4.11	4.97	3.51	complete segregation
	5		4.34	4.02	complete segregation
	4		3.67	4.75	complete segregation
	3		2.96	5.90	3% overlap
	2		2.18	7.99	10% overlap

Furthermore, a number of recent studies have revealed the helical organization of bacterial chromosomes.<sup>93,95,115</sup> A recent computational study shows that a bottle-brush polymer, as shown in Fig. 11(b), is helically organized in a confined, cell-like space<sup>109</sup>; some of the main results are displayed in Fig. 11(c). The observed helical organization is attributed to the interplay between chain stiffening and intrachain packing effects, both induced by side loops. Later, this model has been used as a polymer model of the *Caulobacter crescentus* chromosome.<sup>108</sup>

Each polymer model serves its purpose to some extent. How these models are related with each other is, however, less clear. Also, the applicability of each model remains to be clarified. Further quantitative modelling of bacterial chromosomes will be useful.

**5.2.2 How they interact**—One can use the diagram in Fig. 9(c) to examine the miscibility of two chains (or chromosomes modelled as beads on a string) with varying cylinder-polymer parameters, including those relevant for the *E. coli* chromosome. First, recall  $R_F = \text{const.} \times 1.1N^{3/5}$  (const. = 1 for a linear chain and 0.79 for a ring) and  $\xi = \phi^{-3/4} = [N/\pi(D/2)^2L]^{-3/4}$ .<sup>21</sup> For  $N = 200$ ,  $R_F = 26.4$ . If we choose  $D = 5$ ,  $x = R_F/D = 4.4$ . The blob size  $\xi$  and the fractional overlap distance  $\lambda/L$  depend on the aspect ratio  $r$ . We find that (i) for  $r = 5.6$ ,  $\xi = 2.8$ , and  $\lambda/L = 15\%$  (5%), (ii) for  $r = 4$ ,  $\xi = 2.2$ , and  $\lambda/L = 20\%$  (10%), and (iii) for  $r = 3$ ,  $\xi = 1.8$ , and  $\lambda/L = 30\%$  (20%), where (...) is the fractional overlap distance for the corresponding ring polymer case.

To make this analysis more parallel with our earlier discussion on linear ordering ( $N = 100$ ), in Table 1, we display the fractional overlap distance  $\lambda/L$  for various choices of cylinder-polymer parameters. Compared to the  $N = 200$  case, chain segregation is much enhanced in this case. In other words, chromosomes segregate better if each of them is packed into smaller  $N$ . For  $r = 3$ , the miscibility diagram sug-

gests 10% overlap for linear chains but 3% for ring polymers, rather than 30% and 20%, respectively, for the corresponding  $N = 200$  case. Note that these parameters (both  $N = 100$  and  $N = 200$  with  $r = 3$ ) fall in the acceptable range for the *E. coli* chromosome, as discussed in subsec. 5.1. Also, it has been shown that the presence of crowding agents can facilitate the spatial separation of (ring) polymers in a cylindrical space.<sup>116</sup> In an intuitive picture, the crowding effect can be considered as either bringing the chains closer (enhancing mixing) or compressing each chain into a more tightly packed one (enhancing segregation).<sup>20</sup> In a cylindrical space, the entropy of crowders was shown to favor chain segregation.<sup>116</sup>

It appears that the *E. coli* chromosome is in the spontaneous separation regime, more so for smaller  $N$ . Indeed, the degree of segregation depends on the cylinder-polymer parameters (e.g.,  $L/D$ ,  $D/a$ , and  $N$ ). For fixed  $L/a$  and  $D/a$ , a smaller  $N$  value leads to a smaller  $\lambda/L$  value (better segregation). This may explain much mixing ( $\sim 50\%$ ) in a recent polymer-model analysis with longer chains, each consisting of  $N = 1392$  cylindrical monomers.<sup>94</sup> In a recent review,<sup>92</sup> the aforementioned orderly folding of DNA segments by various proteins is considered to be favorably implicated in chromosome segregation. This assertion appears to be well aligned with the observation that supercoiling or packing defects lead to segregation defects (see Ref.<sup>92</sup> and references therein). However, the picture of orderly-folding as the driver of chromosome segregation and the entropic picture are not mutually exclusive. Along this line, we favor the argument that the entropic segregation force offers a sense of directionality for segregation,<sup>19</sup> which we believe compliments and even strengthens the other picture. Also, as noted earlier, for larger  $N$ , chains mix better. Improper packing can be considered as enlarging  $N$  (weaker segregation). The main difference is through  $\zeta_{||}$ . Similarly to what we expect from cross-linking, orderly-folding can be viewed as shortening  $\zeta_{||}$ , thus enhancing both linear ordering and segregation (see Fig. 9).

To further unravel chain segregation, a quantitative comparison between different polymer models and *in vitro* experiments will be desirable. As a natural extension of the earlier single-chromosome experiment,<sup>14</sup> two chromosomes trapped in a narrow pore can be compressed against each other or manipulated osmotically, in the absence or presence of enzymes that act on the topology of DNA such as type II topoisomerase,<sup>117</sup> which allows DNA strands to cross each other. This will enable one to estimate entropic segregation forces, similar to what was done with simple polymers,<sup>118</sup> to understand better the favorable roles of molecular crowding, or to clarify to what extent chromosome segregation is kinetically limited.

## 6 Conclusions and discussions

Thanks to much effort, a coherent picture of how polymer chains behave under confinement has recently emerged from a few approaches: the blob-scaling approach, Flory theory, simulations, and experiments (see Sec. 2); if constructed with caution, a Flory approach becomes consistent with other approaches. In particular, our review highlights polymer chains as entropic objects. Confinement or a physical constraint can modify polymer chains qualitatively, both single-chain statistics and their segregation properties. It is our view that confinement primarily modifies single-chain properties by reducing their conformational space, which in turn influences the way they interact and segregate (Sec. 4).

Closed cylindrical confinement is particularly intriguing, since it combines both features of open-cylindrical and spherical confinement. This is also relevant to modelling of the bacterial nucleoid. In this case, the notion of blob-chain entropy turns out to be useful for understanding chain segregation (Fig. 8(a)). By segregation, the chains can increase the 'blob-chain' entropy under the right conditions. This is unique to chain molecules and is opposite to what we would expect from a binary mixture of simple molecules. Furthermore, the interdependence between single-chain statistics and chain segregation has been established (Fig. 9).<sup>22</sup> It corrects the earlier scaling picture that linear ordering is required for entropic chain segregation.<sup>7,8</sup> Nevertheless the boundary between various regimes based on the scaling picture are consistent with the numerical data.<sup>22</sup>

Also, there has been a growing interest in understanding the favorable role of molecular crowding, once thought to be 'obvious but under-appreciated,'<sup>81</sup> in organizing a chain molecule especially under confinement (Sec. 3). Indeed the depletion forces induced by molecular crowders are considered to be the main player in condensing the bacterial chromosome.<sup>14,35</sup> Furthermore, the results in Fig. 7 highlight the interplay between crowding and confinement effects. What remains to be further explored is the physical origin of phase-coexistence

observed for bacterial chromosomes in a tube-like space.<sup>14</sup>

In chain segregation and compaction discussed here, entropy is a determining factor (no energy is involved in our athermal systems). In both cases, macroscopic ordering (e.g., segregation and phase separation) emerges from the tendency to maximize microscopic randomness<sup>14</sup> and is favored by the entropy of blob-chains or crowders. Analogous phenomena include the entropic ordering of rod-like molecules into a nematic phase (see for instance Ref.<sup>3</sup>) and the electrostatic attraction between oppositely-charged molecules in solution<sup>119</sup>; in the latter case, the entropy of the surrounding counterions often dominates the electrostatic attraction between the opposite charges.

A few polymer models have been employed to understand quantitatively what was observed with bacterial chromosomes (Sec. 5). In terms of simplicity, a linear or ring polymer model is advantageous over others. Their single chain properties and segregation have been well understood as detailed in this review (see Fig. 9). Beyond the general pictures they offer, however, they have limitations, as discussed in Sec. 5. It will be beneficial to explore more realistic polymer models of bacterial chromosomes (e.g., variations of cross-linked polymers and bottle-brush models in the absence or presence of crowding agents), in concert with our understanding of the physical properties of chromosomes. Of particular interest is how chromosome segregation is influenced by the presence of type II topoisomerase.<sup>117</sup> This effort will enable us to clarify to what extent chromosome segregation is kinetically controlled. Also beyond its impact on equilibrium chain organization discussed in Sec. 3, molecular or macromolecular crowding has profound effects on the dynamics of macromolecules (as in chromosome segregation). For instance, it is considered to be implicated in the sub-diffusive motion of chromosome loci in the (viscoelastic) bacterial cytoplasm.<sup>120</sup> Quantitative modelling of chromosomes will continue to find fascinating problems for polymer/soft matter physics.

## 7 Acknowledgement

This work was supported by NSERC (Canada) (B.-Y.H.), the collaborative research contract funded by Korea Institute of Science and Technology Information (KISTI), and the NRF of Korea: No. 2012R1A1A2007488 (Y.J.). We acknowledge helpful discussions with S. Jun, A. Grosberg, C. Jeon, and J. Kim.

## References

- 1 P. G. de Gennes, *Scaling Concepts in Polymer Physics*, Cornell University Press (Ithaca, NY, 1979).

- 2 M. Rubinstein and R. H. Colby, *Polymer Physics*, Oxford University Press (2003)
- 3 M. Doi and S. F. Edwards, *The Theory of Polymer Dynamics* (Oxford University Press, 1986).
- 4 F. Oosawa, *Polyelectrolytes* (M. Dekker, 1971).
- 5 R. Piazza, *Soft Matter: The stuff that dreams are made of* (Copernicus, 2011).
- 6 F. Brochard and P. G. de Gennes, *J. Chem. Phys.*, 1977, **67**, 52-56.
- 7 M. Daoud and P. G. de Gennes, *J. Phys. (Paris)*, 1977, **38**, 85-93
- 8 F. Brochard and P. G. de Gennes, *J. Phys. (Paris)*, 1979, **40**, L399-L401.
- 9 K. H. Rasmussen, R. Marie, J. M. Lange, W. E. Svendsen, A. Kristensen, and K. U. Mir, *Lab Chip*, 2011, **11**, 1431-1433.
- 10 C. Prinz, J. Tegenfeldt, R. Austin, E. Cox, and J. Sturm, *Lab on a Chip*, 2002, **2**, 207-212.
- 11 T. Su, S. K. Das, M. Xiao, and P. K. Purohit, *PLoS ONE*, 2011, **6**, e16890-1-1-e16890-9.
- 12 W. Reisner et al. *Phys. Rev. Lett.*, 2005, **94**, 196101 (p1-4).
- 13 W. Reisner, J. N. Pedersen, and R. H. Austin, *Rep. Prog. Phys.*, 2012, **75**, 106601 (p1-34).
- 14 J. Pelletier, K. Halvorsen, B.-Y. Ha, R. Paparcone, S. J. Sandler, C. L. Woldringh, W. P. Wong, and S. Jun, *Proc. Nat. Acad. Sci. USA*, 2012, **109**, E2649 - E2656.
- 15 Y. Wang, D. R. Tree, and K. D. Dorfman, *Macromolecules*, 2011, **44**, 6594-6604.
- 16 L. Dai, J. van der Maarel, and P. S. Doyle, *Macromolecules*, 2014, **47**, 2445-2450.
- 17 L. Dai and P. S. Doyle, *Macromolecules*, 2013, **46**, 6336-6344.
- 18 A. Milchev, *J. Phys.: Condens. Matter*, 2011, **23**, 103101-1-103101-24.
- 19 S. Jun and A. Wright, *Nat. Rev. Microbiol.*, 2010, **b**, 600-607.
- 20 See S. Jun, "Polymer Physics for Understanding Bacterial Chromosomes," in *Bacterial Chromatin* (Springer, 2010), edited by R. T. Dame and C. J. Dorman.
- 21 Y. Jung, C. Jeon, J. Kim, H. Jeong, S. Jun, and B.-Y. Ha, *Soft Matter*, 2012, **8**, 2095-2102.
- 22 Y. Jung, J. Kim, S. Jun, and B.-Y. Ha, *Macromolecules*, 2012, **45**, 3256-3262.
- 23 M. Fritsche, S. Li, D. W. Heermann, and P. A. Wiggins, *Nucleic Acids Res.*, 2012, **40**, 972-980.
- 24 A. Cacciuto and E. Luijten, *Phys. Rev. Lett.*, 2006, **96**, 238104 (p1-4).
- 25 Y. Hu, R. Zandi, A. Anavitarte, C. M. Knobler, and W. M. Gelbart, *Biophys. J.*, 2008, **94**, 1428-1436.
- 26 T. Romantsov, I. Fishov and O. Krichevsky, *Biophys. J.*, 2007, **92**, 2875-2884.
- 27 See C. L. Woldringh and T. Odijk in *Organization of the Prokaryotic Genome*, edited by R. L. Charlebois (ASM Press, Washington, D.C. 1999).
- 28 L. Postow, C. D. Hardy, J. Arsuaga, and N. R. Cozzarelli, *Genes Dev.*, 2004, **18**, 1766-1779.
- 29 V. G. Benza, B. Bassetti, K. D. Dorfman, V. F. Scolari, K. Bromek, P. Cicuta, and M. C. Lagomarsino, *Rep. Prog. Phys.*, 2012, **75**, 076602 (20pp).
- 30 Y. Jung, S. Jun, and B.-Y. Ha, *Phys. Rev. E*, 2009, **79**, 061912-1-0619128.
- 31 S. Napolitano, S. Capponi, and B. Vanroy, *Eur. Phys. J. E*, 2013, **36**, 61. p1-37.
- 32 Z. Fakhraai and J. A. Forrest, *Science*, **319**, 600-604 (2008).
- 33 A.-C. Shi and B. Li, *Soft Matter*, 2013, **9**, 1398-1413.
- 34 M. W. Matsen and F. S. Bates, *Macromolecules*, 1996, **29**, 1091-1098.
- 35 J. Kim, C. Jeon, H. Jeong, Y. Jung and B.-Y. Ha, *Soft Matter*, in press, 2015 (DOI: 10.1039/c4sm02198c).
- 36 P. Pincus, *Macromolecules*, 1976, **9**, 386-388.
- 37 J. Kim, C. Jeon, H. Jeong, Y. Jung and B.-Y. Ha, *Soft Matter*, 2013, **9**, 6142-6150.
- 38 P. G. de Gennes, P. Pincus, R. M. Velasco, and F. Brochard, *J. Phys. France*, 1976, **37**, 1461-1473.
- 39 J.-L. Barrat and J. F. Joanny, *Adv. Chem. Phys.*, 1996, **94**, 1-66.
- 40 N. M. Toan, B.-Y. Ha, and D. Thirumalai, "Polyelectrolyte and Polyampholyte Effects in Synthetic and Biological Macromolecules" in *Ionic Interactions in Natural and Synthetic Macromolecules*, Edt. by A. Ciferri and A. Perico (Wiley, 2012).
- 41 S. Jun, A. Arnold, and B.-Y. Ha, *Phys. Rev. Lett.*, 2007, **98**, 128303-1-128303-4.
- 42 A. Cacciuto and E. Luijten, *Nano Lett.*, 2006, **6**, 901-905.
- 43 T. Sakaue, *Macromolecules*, 2007, **40**, 5206-5211.
- 44 S. Jun and B. Mulder *Proc. Natl. Acad. Sci. USA*, 2006, **103**, 12388-12393.
- 45 Y. Liu and B. Chakraborty, *Phys. Biol.*, 2012, **9**, 066005 (5pp).
- 46 A. Arnold, B. Bozorgui, D. Frenkel, B.-Y. Ha, and S. Jun, *J. Chem. Phys.*, 2007, **127**, 164903-1-164903-9.
- 47 S. Jun, D. Thirumalai, and B.-Y. Ha, *Phys. Rev. Lett.*, 2008, **101**, 138101-1-138101-4.
- 48 T. Sakaue and E. Raphaël, *Macromolecules*, 2006, **39**, 2621-2628.
- 49 G. Morrison and D. Thirumalai, *J. Chem. Phys.*, 2005, **122**, 194907-1-194907-5.
- 50 G. Morrison, C. Hyeon, N. M. Toan, B.-Y. Ha, and D. Thirumalai, *Macromolecules*, 2007, **40**, 7343-7353.

- 51 O. A. Saleh, D. B. McIntosh, P. Pincus, and N. Ribeck, *Phys. Rev. Lett.*, 2009, **102**, 068301-1–068301-4.
- 52 P. G. de Gennes, *J. Phys. Lett. (Paris)*, 1975, **36**, L55-L57.
- 53 T. Odijk, *Macromolecules*, 1983, **16**, 1340-1344.
- 54 T. Odijk, *Macromolecules*, 1986, **19**, 2313-2329.
- 55 T. Odijk, *Phys. Rev. E*, 2008, **77**, 060901(R), 1-4.
- 56 J. Z. Y. Chen, *Macromolecules*, 2013, **46**, 9837-9844.
- 57 T. A. Vilgis, *Physics Reports*, 2000, **336**, 167-254.
- 58 P. J. Flory and W. R. Krigbaum, *J. Chem. Phys.*, 1950, **18**, 1086.
- 59 A. Y. Grosberg, P. G. Khalatur, and A. R. Khokhlov, *Makromol. Chem. Rapid Commun.*, 1982, **3**, 709-713.
- 60 A. R. Khokhlov, A. Y. Grosberg, and V. S. Pande, *Statistical Physics of Macromolecules* (Aip Press, 1994).
- 61 J. O. Tegenfeldt et al., *Proc. Nat. Acad. Sci. USA*, 2004, **101**, 10979-10983.
- 62 S. L. Levy, J. T. Mannion, J. Cheng, C. H. Reccius, and H. G. Craighead, *Nano Lett.*, 2008, **8**, 3839-3844.
- 63 L. Onsager, *Ann. NY Acad. Sci.*, 1949, **51**, 627-659.
- 64 L. S. Lerman, *Proc. Nat. Acad. Sci. USA*, 1971, **68**, 1886-1890.
- 65 A. Y. Grosberg, I. Y. Erukhimovitch, and E. I. Shakhnovitch, *Biopolymers*, 1982, **21**, 2413-2432.
- 66 J. A. Valkenburg and C. L. Woldringh, *J. Bacteriol.*, 1984, **160**, 1151-1157.
- 67 J. Stavans and A. Oppenheim, *Phys. Biol.*, 2006, **3**, R1-10.
- 68 R. de Vries, *Biophys. J.*, 2001, **80**, 1186-1194.
- 69 R. de Vries, *Biochimie*, 2010, **92**, 1715-1721.
- 70 S. Cunha, C. L. Woldringh and T. Odijk, *J. Struct. Biol.*, 2001, **136**, 53-66.
- 71 T. Odijk, *Biophys. Chem.*, 1998, **73**, 23-29.
- 72 J. J. Jones, J. R. C. van der Maarel, and P. S. Doyle, *Nano Lett.* 2011, **11**, 5047-5053.
- 73 C. Zhang, P. G. Shao, J. A. van Kan, and J. R. C. van der Maarel, *Proc. Natl. Acad. Sci. USA*, 2009, **106**, 16651-16656.
- 74 M. K. Krotova, V. V. Vasilevskaya, N. Makita, K. Yoshikawa, and A. R. Khokhlov, *Phys. Rev. Lett.*, 2010, **105**, 128302.
- 75 V. V. Vasilevskaya, A. R. Khokhlov, Y. Matsuzawa, and K. Yoshikawa, *J. Chem. Phys.*, 1995, **102**, 6595-6602.
- 76 S. Asakura and F. Oosawa, *J. Chem. Phys.*, 1954, **22**, 1255-1256.
- 77 S. Asakura and F. Oosawa, *J. Polymer Sci.*, 1958, **33**, 183-192.
- 78 H. N. W. Lekkerkerker and R. Tuinier, "Colloids and the Depletion Interaction," *Lecture Notes in Physics*, Vol. 833 (Springer, 2011).
- 79 K. Sneppen and G. Zocchi, *Physics in Molecular Biology* (Cambridge University Press, 2005).
- 80 D. S. Goodsell, *Biochem. Mol. Biol. Education*, 2009, **37**, 325-332.
- 81 R. J. Ellis, *Trends Biochem. Sci.*, 2001, **26**, 597-604.
- 82 S. B. Zimmerman and A. P. Minton, *Annu. Rev. Biophys. Biomol. Struct.*, 1993, **22**, 27-65.
- 83 R. Phillips et al, *Physical Biology of the Cell*, 2nd Edt. (Garland Science, 2012).
- 84 H. Walter and D. E. Brooks, *FEBS Lett.*, 1995, **361**, 135-139.
- 85 D. Marenduzzo, C. Micheletti and P. R. Cook, *Biophys. J.*, 2006, **90**, 3712-3721.
- 86 S. Klump, M. Scott, S. Pedersen and T. Hwa, *Proc. Nat. Acad. Sci. U. S. A.*, 2013, **110**, 16754-16759.
- 87 T. N. Shendruk, M. Bertrand, H. W. de Haan, J. L. Harden and G. W. Slater, arXiv:1407.2850v1 [cond-mat.soft].
- 88 J. L. Jacobsen, *Phys. Rev. E*, 2010, **82**, 051802 (p1-6).
- 89 P. R. Cook and D. Marenduzzo, *J. Cell Biol.*, 2009, **186**, 825-834.
- 90 J. Dorier and A. Stasiak, *Nucleic Acids Res.*, 2009, **37**, 6316-6322.
- 91 D. Račko and P. Cifra, *J. Chem. Phys.*, 2013, **138**, 184904 (p1-7).
- 92 X. Wang, P. M. Llopis, and D. Z. Rudner, *Nat. Rev. Genet.* 2013, **14**, 191-203.
- 93 J. K. Fisher, A. Bourniquel, G. Witz, B. Weiner, M. Prentiss, and N. Kleckner, *Cell*, 2013, **153**, 882-895.
- 94 I. Junier, F. Boccard, O. Espéli, *Nucleic Acids Res.*, 2014, **42**, 1461-1473.
- 95 N. H. Yazdi, C. C. Guet, R. C. Johnson, and J. F. Marko, *Mol. Microbiol.*, 2012, **86**, 1318-1333.
- 96 J. A. C. Valkenburg and C. L. Woldringh, *J. Bacteriol.*, 1984, **160**, 1151-1157.
- 97 K. Bloom and A. Joglekar, *Nature*, 2010, **463**, 446-456.
- 98 V. F. Holmes and N. R. Cozzarelli, *Proc. Natl. Acad. Sci. USA.*, 2000, **97**, 1322-1324.
- 99 A. Worcel and E. Burgi, *J. Mol. Biol.*, 1972, **71**, 127147.
- 100 R. R. Sinden and D. E. Pettijohn, *Proc. Natl. Acad. Sci. USA.*, 1981, **78**, 224-228.
- 101 T. Romantsov, I. Fishov, and O. Krichevsky, *Biophys. J.*, 2007, **92**, 2875-2884.
- 102 X. Wang, X. Liu, C. Possoz, and D. J. Sherratt, *Genes Dev.*, 2006, **20**, 1727-1731.
- 103 X. Liu, X. Wang, R. Reyes-Lamothe, and D. Sherratt, *Mol. Microbiol.*, 2010, **75**, 1090-1097.
- 104 H. Niki, Y. Yamaichi, and S. Hiraga, *Genes & Dev.*, 2000, **14**, 212-223.
- 105 B. Youngren, H. J. Nielsen, S. Jun, and S. Austin, *Genes & Dev.*, 2014, **28**, 71-84.
- 106 F. J. Trueba and C. L. Woldringh, *J. Bacteriology*, 1980,

- 142, 869-878.
- 107 C. Bustamante, J. F. Marko, E. D. Siggia, and S. Y. Smith, *Science*, 1994, **265**, 1599-1600.
- 108 T. B. K. Le, M. V. Imakaev, L. A. Mirny, and M. T. Laub, *Science*, 2013, **342**, 731-734.
- 109 D. Chaudhuri and B. M. Mulder, *Phys. Rev. Lett.*, 2012, **108**, 268305 (p1-4).
- 110 H. J. Nielsen, Y. Li, B. Youngren, F. G. Hansen, S. Austin, *Mol. Microbiol.*, 2006, **61**, 383-393.
- 111 H. J. Nielsen, J. R. Ottensen, B. Youngren, S. J. Austin, F. G. Hansen, *Mol. Microbiol.*, 2006, **62**, 331-338.
- 112 X. Wang, X. Liu, C. Possoz, D. J. Sherratt, *Genes Dev.*, 2006, **20**, 1727-1731.
- 113 P. A. Wiggins, K. C. Cheveralls, J. S. Martin, R. Lintner, and J. Kondev, *Proc. Natl. Acad. Sci. USA.*, 2000, **107**, 4991-4995.
- 114 M. Buenemann and P. Lenz, *PLoS ONE*, 2010, **5**, e138061–e13806-13.
- 115 I. A. Berlatzky, A. Rouvinski, and S. Ben-Yehuda, *Proc. Natl. Acad. Sci.*, 2008, **105**, 4136-4140.
- 116 J. Shin, A. G. Cherstvy, and R. Metzler, *New J. Phys.*, 2014, **16**, 053047 (p1-19).
- 117 J. M. Berger, S. J. Gamblin, S. C. Harrison, and J. C. Wang, *Nature*, 1996, **379**, 225-232.
- 118 Y. Jung and B.-Y. Ha, *Phys. Rev. E*, 2010, **82**, 051926 (p1-5)
- 119 W. M. Gelbart, R. F. Bruinsma, P. A. Pincus, and V. A. Parsegian, *Phys. Today*, 2000, **53**, 38-44.
- 120 S. C. Weber, A. J. Spakowitz, and J. A. Theriot, *Phys. Rev. Lett.*, 2010, **104**, 238102 (p-4).

## A graphical and textual abstract for the Table of contents entry

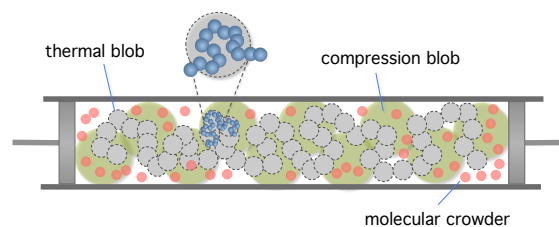


**Fig. 12** A confined polymer in a confined and crowded space.